Distributed Variation Parameter Design for Dynamic Formation Maneuvers with Bearing Constraints

Xiaozhen Zhang, Qingkai Yang, *Member, IEEE,* Jinshuo Lyu, Xinyue Zhao, and Hao Fang, *Member, IEEE*

***Abstract*—The aim of this study is to investigate the problem of cooperative multi-robot variation parameter design for dynamic formation maneuvers with bearing constraints. Notably, scaling and translation are relatively economical bearing-preserving motions in terms of formation changes. Typically, the variation parameters, i.e., the desired scaling size and translation vector, are designed offline a priori, and it is often challenging to dynamically generate the desired formation in response to a changing ambient environment. This paper proposes an online distributed design method to determine the variation parameters of an entire formation. First, local variation policies are generated by the proposed high-order control barrier functions based on received local excitations from the environment. Subsequently, using the distributed average tracking technique, consensus filters are employed to integrate various local variation policies in a weighted-average manner, which ensures that the bearing is maintained in dynamic formation maneuvers. Finally, numerical simulations and experiments are conducted to demonstrate the effectiveness of the proposed method.**

***Note to Practitioners*—This paper is motivated by the neglect of the research on the automatic co-adjustment of the formation variation parameters in most existing formation control schemes, which rely on fixed and pre-defined desired variation parameters (scaling size and translation vector). To address this limitation, this paper suggests an online distributed design method to determine the variation parameters of an entire formation in dynamic ambient environments. The proposed method consists of three parts: 1) By considering received local excitations from the environment as perturbations to asymptotically stable virtual systems, unconstrained local variation policies are generated. 2) By employing high-order control barrier functions, we solve the bounded magnitude constraints for distributed average tracking (DAT) algorithms and the minimum scale constraint for collision avoidance, leading to the generation of constrained local variation policies. 3) By using DAT algorithms, all robots can cooperatively obtain a uniform variation parameter, which is exactly the weighted average of the constrained local variation policies. This ensures that the bearing is maintained in dynamic formation maneuvers. Therefore, the proposed method can be deployed to multi-robot systems in a distributed manner. Finally, numerical simulations and experiments are conducted to demonstrate the feasibility of the proposed method and its potential in industrial applications.**

***Index Terms*—Formation control, formation transformation, multi-robot systems.**

This work was supported in part by the National Key Research and Development Program of China under No. 2022YFA1004703, No. 2022YFB4702000, in part by the Fundamental Research Funds for the Central Universities, in part by the NSFC under Grants 62133002, U1913602, 62088101, 61720106011 and in part by the Shanghai Municipal Science and Technology Major Project (2021SHZDZX0100). *(Corresponding author: Qingkai Yang.)*

Authors are with the National Key Laboratory of Autonomous Intelligent Unmanned Systems (KAIUS), School of Automation, Beijing Institute of Technology, Beijing 100081, China (e-mail: jiaozhen@bit.edu.cn, qingkai.yang@bit.edu.cn, lvjingshuo@bit.edu.cn, xinyue.zhao@bit.edu.cn, fangh@bit.edu.cn).

I. Introduction

COOPERATION of multi-robot systems is a research area with growing interest. Formation control, an important multi-robot cooperative pattern, has been applied to various scenarios, including aerial cooperative transportation [1], forest firefighting [2], surveillance [3], agricultural operations [4], Earth observation [5], and space debris capture [6].

Specific formation motions are often preferred for formation maneuvers under sensing constraints. For example, a significant issue that cannot be ignored in vision-based formation tasks, is the limited detection range of vision sensors [7]-[8]. Bearing-preserving motions are favorable as they retain bearing relationships among pairwise robots [9]. Typically, scaling and translation are two types of bearing-preserving motions.

Translation motion renders the integrated movement of the formation group without changing its geometric shape or size. By adopting a consensus algorithm, formation translation can be achieved based on the leader-follower structure [10]. Time-varying translation is further considered in [11], where the reference translation signal available to all robots is included in the feedforward control term. In [12], Miao *et al.* proposed a formation control method for nonholonomic robots based on the distributed estimation for the leader's states. The authors show that formation tracking errors can converge to zero asymptotically.

Scaling transformation refers to altering the formation size while maintaining its geometric pattern. In [13], Hou *et al.* proposed the dynamic region following formation control (DRFFC) method to control a swarm of robots. In this method, robots are driven into the desired region in a centralized manner. In [15], a distributed scaling control method was proposed for networked robots, in which only two robots were familiar with the desired scale. In [16], given the condition that only two leaders were familiar with the desired formation scale, a distributed estimation-based control method was designed for the remaining robots to automatically form the prescribed formation. The complex Laplacian was used to manage the planar formation scaling problem in [17]-[18], where the leader-follower interactive topology was required to be 2-rooted. Yang *et al.* [19] proposed a scaling control method in the framework of affine formation control. By relying on the estimations of the unknown formation parameter, several formation control laws were developed with two leaders [20]-[21] and a single leader [22] familiar with the desired formation size. Time delays are additionally considered in [23], where the authors designed a predictive

observer-based control scheme for formation stabilization. Onuoha *et al.* [24] extended the affine formation-based scaling control method to triple-integrator systems, and proposed a sampled-data controller to deal with practical periodic intervals limitation. Zhao and Zelazo [25] proposed a bearing-based method for realizing the formation scale. Uncertainties and input saturation were studied in [26]. In [27], the authors revealed that triangulations are infinitesimally shape-similar. By invoking this property, the bearing-only control method was proposed to maintain triangulations for planar formation keeping, where the formation size is determined by two robots. Although many translation and scaling control methods have been developed, determining or designing the formation scaling size and translation motions in a distributed manner to accommodate dynamic environments remains a challenging problem.

Notably, for every single robot, obtaining local variation policies according to local environmental excitations is straightforward, but uniform variation parameters are necessary for the entire formation maneuver. If we treat local variation policies as reference signals of the distributed average tracking (DAT) algorithm, it is possible to obtain uniform formation variation parameters, which are exactly the weighted average of the local variation policies. Linear DAT algorithms have been applied to reach the average consensus of multi-robot systems with bounded errors [28]. By employing the signum function, nonsmooth DAT algorithms have been proposed to track the average of multiple time-varying reference signals with bounded derivatives [29]-[30]. By combining potential functions, the DAT algorithm was used to track the average of a class of refer velocity signals and realize obstacle avoidance for a swarm of robots [31]. In [32], Chen *et al.* presented the connection between the DAT and DRFFC methods [13], demonstrating that the DAT-based DRFFC method could exhibit richer formation behavior that facilitates obstacle avoidance. However, reference signals (local variation policies) often must to be constrained to some domain for DAT algorithms, such as those utilizing bounded derivatives [33]-[34] or bounded accelerations [35]. Moreover, in practical formation tasks, local variation policies also require minimum-scale constraints to avoid collisions. Therefore, it is important to ensure that local variation policies satisfy the desired constraints.

The control barrier function (CBF) was introduced to transform safety constraints into state-dependent linear inequality constraints on the inputs [36]. In [37]-[38], the high-order CBF (HOCBF) was proposed to deal with arbitrarily high relative degree constraints. [40] stipulated a sufficient condition for the control-sharing property of multiple CBFs, which can be used to analyze the conflict between CBFs. The designer must exercise caution when designing specific forms of the desired constraints of local variation policies to constitute CBFs because unreasonable constraint expressions often lead to conflicts and loss of the control-sharing property.

This paper addresses the challenges of dynamically generating desired formations in response to changing ambient environments, which has been rarely studied in previous research. Typically, the desired formations are given a priori. The lack of automatic co-adjustment of formation variation parameters limits the flexibility and adaptability of formation behaviors. To address this issue, we propose an online distributed design method for determining the scaling and translation parameters of an entire formation. The proposed method can maintain the bearing relationships among pairwise robots during dynamic maneuvers, and significantly increase the flexibility and practicability of formation behaviors. First, the excitation vectors received from the environment are regarded as external perturbations to asymptotically stable virtual triple-integrator systems, which can generate unconstrained local variation policies. Second, by employing HOCBFs, the bounded magnitude constraint for DAT algorithms and the minimum-scale constraint for collision avoidance are solved. We demonstrate that the constituted HOCBFs experience no conflicts, implying that HOCBFs have the control-sharing property. Next, DAT-based consensus filters are proposed to integrate constrained local variation policies in a weighted-average manner. All the robots can obtain uniform formation scaling and translation parameters in a distributed manner. Consequently, the bearing constraints among the different robots are naturally maintained.

The main contributions of this study are summarized as follows:

1) By using projection operations, the robots' environmental excitation vectors are converted to direct excitation forms of formation variation. Compared with the formation maneuver methods with pre-defined parameters [21]-[25], the formation parameters herein can be self-adjusted in response to the environment, so it is significantly more flexible and practical.
2) The HOCBFs are designed to solve the constraints of local variation policies. The control-sharing property of the HOCBFs is rigorously proved. In this study, the considered constraints in CBFs do not contain bounded functions, which makes the input constraints highly coupled with states. Therefore, the analysis of the control-sharing property is more complex and challenging than [40]-[41], where the boundedness of $\sin(\cdot)$ and $\cos(\cdot)$ functions is utilized to estimate the inputs constraints without state couplings.
3) DAT-based consensus filters, which can integrate local variation policies in a weighted-average manner, are proposed to obtain uniform formation variation parameters. This approach ensures that bearings will be preserved in the resulting formation maneuvers. Different from the applications in [31]-[32], this paper first uses DAT algorithms in the formation variation parameter decision problem. The tracking ability of the DAT algorithms on the mean is used to achieve the weighted average required for cooperative decision-making. We expand the possible applications of the DAT algorithm to formation tasks.

The remainder of this paper is organized as follows. First, some preliminaries and the formation problem are presented in Section II. The design method for the formation scaling parameters is described in Section III. Following the steps

described in Section III, the translation parameters are described in Section IV. Finally, the simulations and experiments conducted to verify the proposed design method are discussed in Section V.

II. Preliminaries and Problem Description

TABLE I
List of Key Notations and Variables

Symbol	Quantity
$\boldsymbol{p}^* \in \mathbb{R}^3$	Reference trajectory
$\boldsymbol{r}_i^* \in \mathbb{R}^3$	Nominal formation of ith robot
$\boldsymbol{p}_i \in \mathbb{R}^3$	Position of ith robot
$\boldsymbol{f}_i \in \mathbb{R}^3$	Environmental excitation for ith robot
$\rho_i \in \mathbb{R}$	Local scaling policy of ith robot
$v_{\kappa i} \in \mathbb{R}$	Scaling excitation of ith robot
$\mu_{\kappa i} \in \mathbb{R}$	Input for the local scaling policy dynamics
$\kappa* \in \mathbb{R}$	Nominal scale
$\kappa_{\min} \in \mathbb{R}$	Minimum scale
$k_{\kappa f} \in \mathbb{R}^+$	Gain for scaling excitation
$k_\kappa, a_\kappa, b_\kappa \in \mathbb{R}^+$	Control gains for local scaling policy
$\varepsilon_\kappa \in \mathbb{R}^+$	Maximum magnitude of local scaling policy
$h_1 : \mathbb{R}^3 \to \mathbb{R}$	Magnitude constraints of local scaling policy
$h_2 : \mathbb{R} \to \mathbb{R}$	Minimum constraints of local scaling policy
$\delta_{1\kappa}, \delta_{2\kappa}, \delta_{3\kappa} \in \mathbb{R}^+$	Parameters of class $\mathcal{K}$ functions for h_1
$\gamma_\kappa \in \mathbb{R}^+$	Parameter of the class $\mathcal{K}$ function for h_2
$\kappa_i \in \mathbb{R}$	Scaling parameter of ith robot
$u_{\kappa i} \in \mathbb{R}$	Input for the scaling parameter dynamics
$\varphi_\kappa, \pi_\kappa \in \mathbb{R}^+$	Control gains for scaling parameter
$\boldsymbol{w}_i \in \mathbb{R}^3$	Local translation policy of ith robot
$\boldsymbol{u}_{qi} \in \mathbb{R}^3$	Input for the translation parameter dynamics
$k_{qf} \in \mathbb{R}^+$	Gain for translation excitation
$k_q, a_q, b_q \in \mathbb{R}^+$	Control gains for local translation policy
$\varepsilon_{\boldsymbol{q}} \in \mathbb{R}^+$	Maximum magnitude of local translation policy
$h_3 : \mathbb{R}^9 \to \mathbb{R}$	Magnitude constraints of local translation policy
$\gamma_q \in \mathbb{R}^+$	Parameter of the class $\mathcal{K}$ function for h_3
$\boldsymbol{q}_i \in \mathbb{R}^3$	Translation parameter of ith robot
$\boldsymbol{\mu}_{qi} \in \mathbb{R}^3$	Input for the local translation policy dynamics
$\varphi_q, \pi_q \in \mathbb{R}^+$	Control gains for translation parameter

A. Control Barrier Function

This function is considered a general affine control system:

$$\dot{\boldsymbol{x}} = f(\boldsymbol{x}) + g(\boldsymbol{x})\boldsymbol{u} \quad \boldsymbol{x}(t) \in \mathbb{R}^c. \tag{1}$$

Function $b(\boldsymbol{x}) : \mathbb{R}^c \to \mathbb{R}$ is continuously m^{th} order differentiable.

Definition 1: (Relative degree [38],[40]) The relative degree of $b(\boldsymbol{x})$ with respect to system (1) is the number of times needed to differentiate it along the system dynamics until the control $\boldsymbol{u}$ is explicitly demonstrated.

First, a series of functions $\theta_i(\boldsymbol{x}) : \mathbb{R}^c \to \mathbb{R}$ is defined as follows:

$$\begin{aligned}
\theta_0(\boldsymbol{x}) &:= b(\boldsymbol{x}), \\
\theta_1(\boldsymbol{x}) &:= \dot{\theta}_0(\boldsymbol{x}) + \alpha_1(\theta_0(\boldsymbol{x})), \\
&\vdots \\
\theta_m(\boldsymbol{x}) &:= \dot{\theta}_{m-1}(\boldsymbol{x}) + \alpha_m(\theta_{m-1}(\boldsymbol{x})),
\end{aligned}$$

where $\alpha_m(\cdot)$ denotes the class $\mathcal{K}$ function of its argument.

According to the defined functions, a series of invariant sets can be defined as follows:

$$\begin{aligned}
\mathcal{C}_1 &:= \left\{\boldsymbol{x} \in \mathbb{R}^d : \theta_0(\boldsymbol{x}) \geq 0\right\}, \\
\mathcal{C}_2 &:= \left\{\boldsymbol{x} \in \mathbb{R}^d : \theta_1(\boldsymbol{x}) \geq 0\right\}, \\
&\vdots \\
\mathcal{C}_m &:= \left\{\boldsymbol{x} \in \mathbb{R}^d : \theta_{m-1}(\boldsymbol{x}) \geq 0\right\}.
\end{aligned}$$

Function $b(\boldsymbol{x})$ with relative degree m is a CBF (HOCBF, if $m > 1$), if there exist differentiable class $\mathcal{K}$ functions $\alpha_1(\cdot)$, $\alpha_2(\cdot)$ ... $\alpha_m(\cdot)$, such that

$$\begin{aligned}
L_f^m b(\boldsymbol{x}) + L_g L_f^{m-1} b(\boldsymbol{x})\boldsymbol{u} + \frac{\partial^m b(\boldsymbol{x})\boldsymbol{u}}{\partial t^m} \\
+ O(b(\boldsymbol{x})) + \alpha_m(\theta_{m-1}(\boldsymbol{x})) \geq 0,
\end{aligned} \tag{2}$$

for all $\boldsymbol{x} \in \mathcal{C}_1 \bigcap \mathcal{C}_2 \bigcap, ..., \bigcap \mathcal{C}_m$, where $O(\cdot)$ denotes the remaining Lie derivatives along f and the partial derivatives with respect to t with a degree less than or equal to $m-1$.

Lemma 1 ([38] Theorem 5): If the initial value is $\boldsymbol{x}(t_0) \in \mathcal{C}_1 \bigcap \mathcal{C}_2 \bigcap, ..., \bigcap \mathcal{C}_m$, and if any Lipschitz continuous controller $\boldsymbol{u}$ satisfies (2), set $\mathcal{C}_1 \bigcap \mathcal{C}_2 \bigcap, ..., \bigcap \mathcal{C}_m$ is forward invariant for system (1).

B. Graph Theory

A graph $\boldsymbol{\mathcal{G}}$ is a pair $(\boldsymbol{\mathcal{V}}, \boldsymbol{\mathcal{E}})$, where $\boldsymbol{\mathcal{V}} = \{v_1, ..., v_n\}$ is a non-empty finite set of nodes and $\boldsymbol{\mathcal{E}} \subseteq \boldsymbol{\mathcal{V}} \times \boldsymbol{\mathcal{V}}$ is a set of ordered pairs of nodes, called edges. An edge (v_j, v_i) represents the communication path from node v_j to node v_i.

The adjacency matrix is $\boldsymbol{\mathcal{A}} = [a_{ij}] \in \mathbb{R}^{n \times n}$, where $a_{ij} = 1$, if $(v_j, v_i) \in \boldsymbol{\mathcal{E}}$, and $a_{ij} = 0$, if $(v_j, v_i) \notin \boldsymbol{\mathcal{E}}$. In general, $a_{ii} = 0$ is defined. The set $\boldsymbol{\mathcal{N}}_i = \left\{j \in \boldsymbol{\mathcal{V}} : \quad (v_j, v_i) \in \boldsymbol{\mathcal{E}}\right\}$ contains all neighbors of node v_i.

The Laplacian matrix is $\boldsymbol{\mathcal{L}} = [l_{ij}] \in \mathbb{R}^{n \times n}$, where $l_{ij} = -a_{ij}$, if $i \neq j$ and $l_{ij} = \sum_{j \in \boldsymbol{\mathcal{N}}_i} a_{ij}$, if $i = j$. The incidence matrix is $\boldsymbol{\mathcal{H}} = [h_{ik}] \in \mathbb{R}^{|\boldsymbol{\mathcal{V}}| \times |\boldsymbol{\mathcal{E}}|}$, where

$$h_{ik} = \begin{cases} 1 & \text{if } v_i \text{ is the is the head of } k\text{th edge} \\ -1 & \text{if } v_i \text{ is the is the end of } k\text{th edge} \\ 0 & \text{otherwise} \end{cases}.$$

The incidence matrix and Laplacian matrix satisfy $\boldsymbol{\mathcal{L}} = \boldsymbol{\mathcal{H}}\boldsymbol{\mathcal{H}}^{\mathrm{T}}$.

C. Problem Description

Assumption 1: The interactive graph $\boldsymbol{\mathcal{G}}$ among robots is connected and undirected.

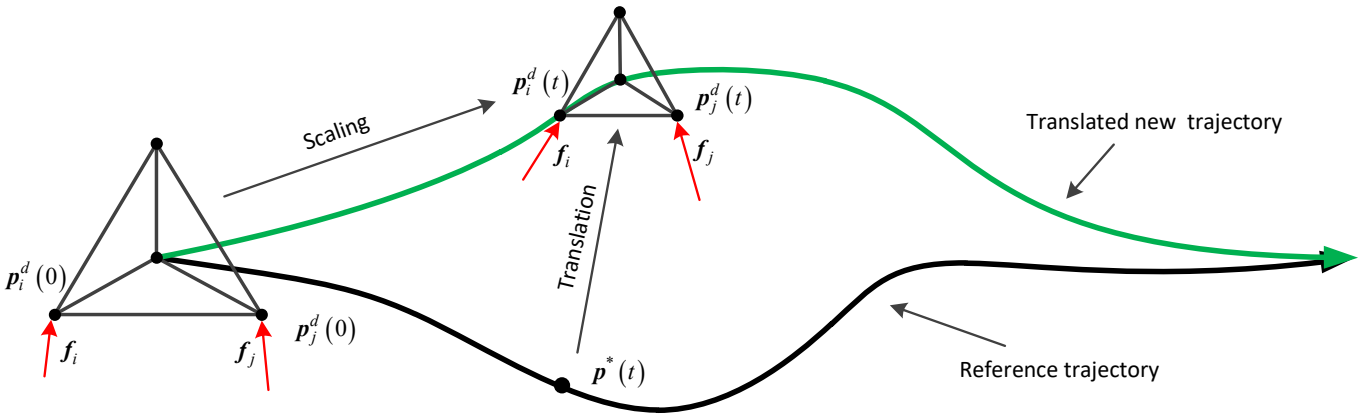

Fig. 1. Formation maneuvers with scaling and translation.

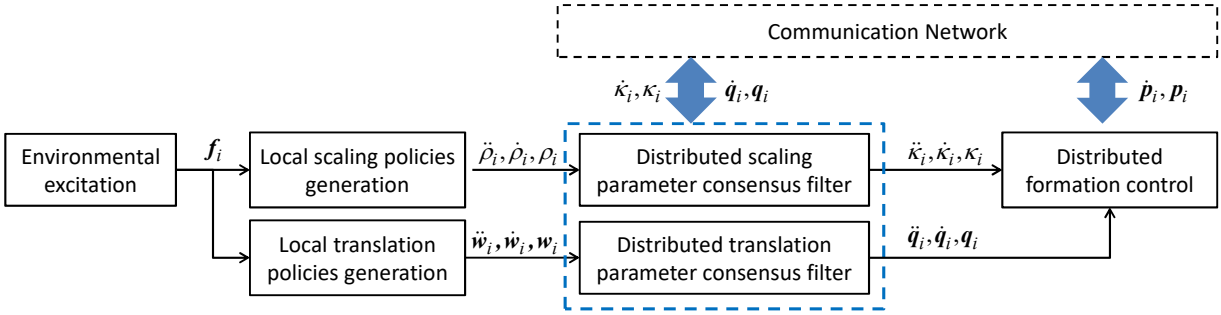

Fig. 2. Framework of the proposed distributed formation scaling and translation parameters design method with formation control.

The connectivity of the graph is the basic assumption of networked systems [10]. Further, when using wireless communication, it is generally possible to establish bilateral communication if the wireless signals of two robots are reachable, so it is assumed that the graph is also undirected. Assumption 1 is consistent with the practical cooperative robotic systems.

The aim of this study is to investigate the problem of designing formation variation parameters for dynamic maneuvers with bearing constraints. Note that only bearing-preserving motions, including scaling and translation, are permitted. It is considered that n robots exhibit double-integrator dynamics:

$$\ddot{\boldsymbol{p}}_i = \boldsymbol{u}_i, \tag{3}$$

where $\boldsymbol{p}_i \in \mathbb{R}^3$ denotes the Cartesian position of the ith robots. First, some definitions are provided herein.

Reference trajectory: The reference trajectory $\boldsymbol{p}^*(t) \in \mathbb{R}^3$ is a given trajectory of the formation, which is known to all robots. It can be determined by a specific mission or some path-planning methods.

Nominal formation: $\boldsymbol{r}^* = \left[(\boldsymbol{r}_1^*)^{\mathrm{T}} \quad \cdots \quad (\boldsymbol{r}_n^*)^{\mathrm{T}}\right]^{\mathrm{T}} \in \mathbb{R}^{3n}$ is the nominal formation with respect to the reference trajectory $\boldsymbol{p}^*$, which is a typical constant geometric pattern. The ith robot is familiar with its own nominal formation and that of its neighbors $\{\boldsymbol{r}_j^*\}_{j\in\mathcal{N}_i\cup\{i\}}$.

Each robot can receive a local excitation vector $\boldsymbol{f}_i(t) \in \mathbb{R}^3$, which represents the locally recognized formation variation tendency. These excitation vectors can be different, time-varying, and discontinuous. $\boldsymbol{f}_i(t)$ is assumed to satisfy the following assumption:

Assumption 2: $\boldsymbol{f}_i(t)$ is bounded, satisfying $||\boldsymbol{f}_i(t)||_2 < \sigma$, where σ is a finite positive value.

The computation of $\boldsymbol{f}_i(t)$ is carried out by the robot itself in response to the environment, and the robot can restrict $\boldsymbol{f}_i(t)$ in the computational algorithm. Therefore, the boundedness of $\boldsymbol{f}_i(t)$ is achievable.

In the proposed method, the entire formation can be scaled from the nominal formation and translated from the reference trajectory. Each robot maintains a formation scaling parameter $\kappa_i(t) \in \mathbb{R}$ with respect to the nominal formation and a translation parameter $\boldsymbol{q}_i(t) \in \mathbb{R}^3$ with respect to the reference trajectory.

To achieve dynamic formation maneuvers with bearing constraints, robots must reach a consensus on the scaling and translation parameters. Therefore, the primary objective of this study is to cooperatively generate the formation scaling and translation transformations according to the local excitation vectors $\{\boldsymbol{f}_i(t)\}_{i=1}^n$, such that

$$\lim_{t\to\infty} \kappa_i(t) - \kappa_j(t) = 0,$$
$$\lim_{t\to\infty} \boldsymbol{q}_i(t) - \boldsymbol{q}_j(t) = 0.$$

Note that we will omit argument t when it is clear that we are referring to $\rho_i(t)$, $\boldsymbol{w}_i(t)$, $\kappa_i(t)$, $\boldsymbol{q}_i(t)$, and $\boldsymbol{f}_i(t)$.

For clarity, the notations and variables are listed in Table 1.

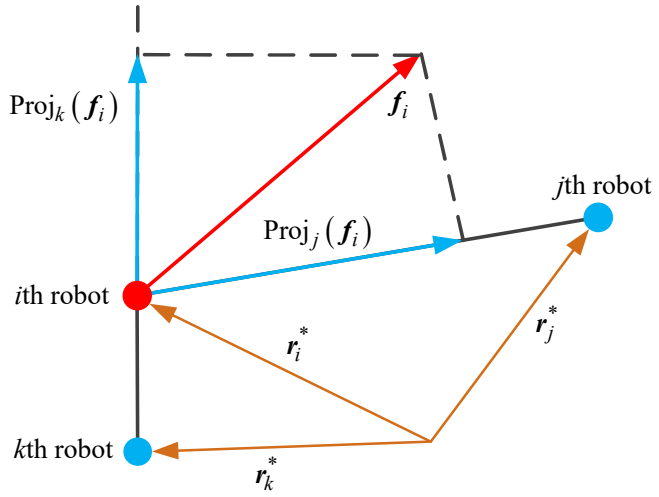

Fig. 3. The projection of $\boldsymbol{f}_i$ along the edges of the nominal formation. For the ith robot of this figure, $\text{Proj}_j\left(\boldsymbol{f}_i\right)^{\mathrm{T}}\left(\boldsymbol{r}_j^*-\boldsymbol{r}_i^*\right)>0$ and $\text{Proj}_k\left(\boldsymbol{f}_i\right)^{\mathrm{T}}\left(\boldsymbol{r}_k^*-\boldsymbol{r}_i^*\right)<0$. Thereby, it has $j\in\hat{\boldsymbol{\mathcal{N}}}_i$ and $k\notin\hat{\boldsymbol{\mathcal{N}}}_i$.

The framework of the proposed method is illustrated in Fig. 2. First, each robot generates the local scaling $\rho_i\in\mathbb{R}$ and translation $\boldsymbol{w}_i\in\mathbb{R}^3$ policy, according to the local excitation vector $\boldsymbol{f}_i$. Owing to the difference in $\boldsymbol{f}_i$, the generated local variation policies are also different. Then, the developed DAT-based consensus filters integrate the diverse local variation policies to reach an agreement in a weighted-average manner. Consequently, the desired position $\boldsymbol{p}_i^d=\boldsymbol{p}^*+\boldsymbol{q}_i+\kappa_i\boldsymbol{r}_i^*$ is provided to the distributed formation controller of the robots.

By using an appropriate $\boldsymbol{f}_i$, the formation can be transformed to realize obstacle avoidance, gathering, and other behaviors. The remainder of this paper introduces our design methods for determining the formation variation parameters.

III. Formation Scaling Parameters Design

This section describes the manner in which the formation scaling parameters reach an agreement for bearing-preserving maneuvers, as illustrated in Fig. 2. First, the local excitation vector $\boldsymbol{f}_i$ is transformed into a formation scaling excitation, generating a nominal control for the local scaling policy without constraints. Then, by using the elaborately designed forms of the bounded magnitude and minimum-scale constraints, we constitute HOCBFs to generate constrained local scaling policies. Finally, a developed consensus filter ensures that the formation scaling parameters reach an agreement, which is exactly the weighted average of the constrained local scaling policies.

A. Unconstrained Local Scaling Policy Design

The dynamics of the local scaling policy $\rho_i\in\mathbb{R}$ are governed by the following virtual triple-integrator system (4):

$$\dddot{\rho}_i=\mu_{i\kappa},\tag{4}$$

where $\mu_{i\kappa}$ is the input.

The influence of $\boldsymbol{f}_i$ on the formation scaling excitation is defined as

$$v_{i\kappa}=\begin{cases}\dfrac{1}{\left|\hat{\boldsymbol{\mathcal{N}}}_i\right|}\displaystyle\sum_{j\in\hat{\boldsymbol{\mathcal{N}}}_i}\dfrac{\left\|\text{Proj}_j\left(\boldsymbol{f}_i\right)\right\|_2}{\left\|\boldsymbol{r}_j^*-\boldsymbol{r}_i^*\right\|_2} & \hat{\boldsymbol{\mathcal{N}}}_i\neq\varnothing\\ 0 & \hat{\boldsymbol{\mathcal{N}}}_i=\varnothing\end{cases}\tag{5}$$

with

$$\hat{\boldsymbol{\mathcal{N}}}_i=\left\{j\in\boldsymbol{\mathcal{N}}_i\ :\ \text{Proj}_j\left(\boldsymbol{f}_i\right)^{\mathrm{T}}\left(\boldsymbol{r}_j^*-\boldsymbol{r}_i^*\right)>0\right\},$$

$$\text{Proj}_j\left(\boldsymbol{f}_i\right)=\frac{\boldsymbol{f}_i^{\mathrm{T}}\left(\boldsymbol{r}_j^*-\boldsymbol{r}_i^*\right)}{\left\|\boldsymbol{r}_j^*-\boldsymbol{r}_i^*\right\|_2^2}\left(\boldsymbol{r}_j^*-\boldsymbol{r}_i^*\right),$$

where only the formation scale reduction is considered in $\hat{\boldsymbol{\mathcal{N}}}_i$. $\text{Proj}_j\left(\boldsymbol{f}_i\right)$ represents the projection of $\boldsymbol{f}_i$ along the edge of the nominal formation $\left(\boldsymbol{r}_j^*-\boldsymbol{r}_i^*\right)$. These relationships are illustrated in Fig. 3.

The environmental excitation $\boldsymbol{f}_i$ is transformed into the formation scaling excitation $v_{i\kappa}$ by (5). The local scaling policy should change the formation scale size according to $v_{i\kappa}$ and restore it to the nominal scale $\kappa^*:=1$ when $v_{i\kappa}=0$. The following unconstrained nominal control law is developed for (4):

$$\mu_{i\kappa}=-k_\kappa s_{i\kappa}-a_\kappa\ddot{\rho}_i-b_\kappa\dot{\rho}_i+k_{\kappa f}v_{i\kappa},\tag{6}$$

where $k_\kappa>0$, $a_\kappa>1$, and $b_\kappa>0$; $k_{\kappa f}>0$ is a gain that adjusts the effect of $\boldsymbol{f}_i$. A larger $k_{\kappa f}$ allows the scaling excitation to more easily scale the formation. $s_{i\kappa}$ is the sliding mode surface designed as follows:

$$s_{i\kappa}=\ddot{\rho}_i+a_\kappa\dot{\rho}_i+b_\kappa\left(\rho_i-\kappa^*\right).\tag{7}$$

Theorem 1: Under Assumption 2, with any $k_\kappa>0$, $a_\kappa>1$, $b_\kappa>0$, and $k_{\kappa f}>0$ for the dynamics (4) and control (6), if $v_{i\kappa}=0$, then $(\ddot{\rho}_i,\dot{\rho}_i,\rho_i)$ converges to $(0,0,\kappa^*)$. If $v_{i\kappa}\neq 0$, then a local scaling policy with the effect of $v_{i\kappa}$ or $\boldsymbol{f}_i$ is generated.

Proof: See Appendix A. ■

B. Constrained Local Scaling Policy Design

An unconstrained nominal control for local scaling dynamics (4) is obtained using (6). The following constraints are considered:

$$h_1\left(\rho_i,\dot{\rho}_i,\ddot{\rho}_i\right)=\varepsilon_\kappa^2-\left[\ddot{\rho}_i+a_\kappa\dot{\rho}_i+b_\kappa\left(\rho_i-\kappa_{\min}\right)\right]^2\geq 0,\tag{8}$$

$$h_2\left(\rho_i\right)=\rho_i-\kappa_{\min}\geq 0,\tag{9}$$

where $\varepsilon_\kappa>0$ and $\kappa^*>\kappa_{\min}>0$ can be designed. $\kappa_{\min}$ represents the feasible minimum formation scale. The constraint $h_1\left(\rho_i,\dot{\rho}_i,\ddot{\rho}_i\right):\mathbb{R}^3\to\mathbb{R}$ is designed for the consensus filter, as will be described in the next subsection. The constraint $h_2\left(\rho_i\right):\mathbb{R}\to\mathbb{R}$ is designed to constrain the generated formation scale ρ_i to no less than the minimum scale $\kappa_{\min}$ for safety. Constraints (8) and (9) require that ρ_i, $\dot{\rho}_i$, and $\ddot{\rho}_i$ are always in the forward invariant set $\mathcal{C}_\kappa$, defined as

$$\mathcal{C}_\kappa:=\left\{\begin{bmatrix}\rho_i & \dot{\rho}_i & \ddot{\rho}_i\end{bmatrix}^{\mathrm{T}}\in\mathbb{R}^3:h_1\left(\rho_i,\dot{\rho}_i,\ddot{\rho}_i\right)\geq 0,h_2\left(\rho_i\right)\geq 0\right\}.\tag{10}$$

We will omit arguments ρ_i, $\dot{\rho}_i$, and $\ddot{\rho}_i$, when it is clear that we are referring to $h_1(\rho_i, \dot{\rho}_i, \ddot{\rho}_i)$ and $h_2(\rho_i)$. The CBFs are constructed as follows to solve the constraint problem. For h_1, we consider the following series of functions:

$$\begin{aligned}
\xi_0 :=& h_1, \\
\xi_1 :=& \dot{\xi}_0 + \gamma_\kappa \xi_0 \\
=& \dot{h}_1 + \gamma_\kappa h_1 \\
=& -2\left[\ddot{\rho}_i + a_\kappa \dot{\rho}_i + b_\kappa(\rho_i - \kappa_{\min})\right](a_\kappa \ddot{\rho}_i + b_\kappa \dot{\rho}_i) \\
& -2\left[\ddot{\rho}_i + a_\kappa \dot{\rho}_i + b_\kappa(\rho_i - \kappa_{\min})\right]\mu_{i\kappa} \\
& + \gamma_\kappa\left\{\varepsilon_\kappa^2 - \left[\ddot{\rho}_i + a_\kappa \dot{\rho}_i + b_\kappa(\rho_i - \kappa_{\min})\right]^2\right\},
\end{aligned} \tag{11}$$

where $\gamma_\kappa \xi_0$ is a class $\mathcal{K}$ function with $\gamma_\kappa > 0$.

Similarly, for h_2, we consider the following series of functions:

$$\begin{aligned}
\zeta_0 :=& h_2, \\
\zeta_1 :=& \dot{\zeta}_0 + \delta_{1\kappa}\zeta_0 \\
=& \dot{\rho}_i + \delta_{1\kappa}(\rho_i - \kappa_{\min}), \\
\zeta_2 :=& \dot{\zeta}_1 + \delta_{2\kappa}\zeta_1 \\
=& \ddot{\rho}_i + \delta_{1\kappa}\dot{\rho}_i + \delta_{2\kappa}\left[\dot{\rho}_i + \delta_{1\kappa}(\rho_i - \kappa_{\min})\right], \\
\zeta_3 :=& \dot{\zeta}_2 + \delta_3 \zeta_2 \\
=& \mu_{i\kappa} + \delta_{1\kappa}\ddot{\rho}_i + \delta_{2\kappa}(\ddot{\rho}_i + \delta_{1\kappa}\dot{\rho}_i) \\
& + \delta_{3\kappa}\left\{\ddot{\rho}_i + \delta_{1\kappa}\dot{\rho}_i + \delta_{2\kappa}\left[\dot{\rho}_i + \delta_{1\kappa}(\rho_i - \kappa_{\min})\right]\right\} \\
=& \mu_{i\kappa} + (\delta_{1\kappa} + \delta_{2\kappa} + \delta_{3\kappa})\ddot{\rho}_i \\
& + (\delta_{2\kappa}\delta_{1\kappa} + \delta_{3\kappa}\delta_{1\kappa} + \delta_{3\kappa}\delta_{2\kappa})\dot{\rho}_i \\
& + \delta_{3\kappa}\delta_{2\kappa}\delta_{1\kappa}(\rho_i - \kappa_{\min}),
\end{aligned} \tag{12}$$

where $\delta_{1\kappa}\zeta_0$, $\delta_{2\kappa}\zeta_1$, and $\delta_3\zeta_2$ are class $\mathcal{K}$ functions with $\delta_{o\kappa} > 0$, $o \in \{1, 2, 3\}$.

The relative degrees of h_1 and h_2 with respect to system (4) are 1 and 3, respectively. Hence, h_2 is a HOCBF that satisfies $\zeta_3 \geq 0$.

According to Lemma 1, to satisfy the constraints (8) and (9), the modified control $\mu_{i\kappa}$ from a nominal control $\mu_{i\kappa}^{\text{ref}}$ can be obtained by the following HOCBF quadratic programming (QP):

$$\begin{cases} \mu_{i\kappa} = \arg\min \dfrac{1}{2}\left(\mu_{i\kappa} - \mu_{i\kappa}^{\text{ref}}\right)^2 \\ s.t. \quad \xi_1 \geq 0 \\ \qquad \zeta_3 \geq 0 \end{cases}. \tag{13}$$

where

$$\mu_{i\kappa}^{\text{ref}} = -k_\kappa s_{i\kappa} - a_\kappa \ddot{\rho}_i - b_\kappa \dot{\rho}_i + k_{\kappa f} v_{i\kappa}$$

is the unconstrained nominal control proposed in (6).

Note that both ξ_1 and ζ_3 are designed for the same control input $\mu_{i\kappa}$. The existence of the control $\mu_{i\kappa}$ must be analyzed. Alternatively, h_1 and h_2 exhibit the control-sharing property [40].

Theorem 2: If the selected parameters of class $\mathcal{K}$ functions in (11) and (12) satisfy (14), then the control $\mu_{i\kappa}$ in (13) for the dynamics (4) must exist with constraints $\xi_1 \geq 0$ and $\zeta_3 \geq 0$.

$$\begin{cases} 1 = \delta_{1\kappa} + \delta_{2\kappa} + \delta_{3\kappa} - a_\kappa - 0.25\gamma_\kappa \\ a_\kappa = \delta_{2\kappa}\delta_{1\kappa} + \delta_{3\kappa}\delta_{1\kappa} + \delta_{3\kappa}\delta_{2\kappa} - b_\kappa - 0.25\gamma_\kappa a_\kappa \\ b_\kappa = \delta_{3\kappa}\delta_{2\kappa}\delta_{1\kappa} - 0.25\gamma_\kappa b_\kappa \end{cases}. \tag{14}$$

Proof: See Appendix B. ■

Remark 1: Typically, it is difficult to solve a system of nonlinear equations (14) using algebraic methods. When using numerical methods, certain parameters can be fixed. For example, in our simulation, $\varepsilon_\kappa = 1.5$, $\gamma_\kappa = 1$, and $\delta_{1\kappa} = 1.5$ are fixed. Then, one feasible solution is obtained (see Section V-A).

C. Distributed Scaling Consensus Filter

Diverse local scaling policies are generated using (4), (6), and (13). Further, a unique formation scaling parameter should be provided for bearing-preserving motions. The formation scaling parameter is governed by the following dynamics:

$$\ddot{\kappa}_i = u_{i\kappa}. \tag{15}$$

A DAT-based consensus filter is presented in (16), which can integrate local scaling policies in a weighted-average manner.

$$\begin{aligned}
u_{i\kappa} =& \ddot{\rho}_i - a_\kappa(\dot{\kappa}_i - \dot{\rho}_i) - b_\kappa(\kappa_i - \rho_i) \\
& - \varphi_\kappa \sum_{j \in \boldsymbol{\mathcal{N}}_i} \operatorname{sgn}(\kappa_i - \kappa_j) - \pi_\kappa \sum_{j \in \boldsymbol{\mathcal{N}}_i} \operatorname{sgn}(\dot{\kappa}_i - \dot{\kappa}_j),
\end{aligned} \tag{16}$$

where the following conditions should be satisfied:

$$\begin{cases} \varphi_\kappa > n(n-1)\varepsilon_\kappa \\ \pi_\kappa > \varphi_\kappa + n(n-1)\varepsilon_\kappa \end{cases}. \tag{17}$$

Theorem 3: Under Assumption 1, if (17) is satisfied, the DAT-based consensus filter (16) can enforce formation scaling parameters with dynamics (15) to reach a consensus, which is exactly the weighted average of constrained local scaling policies.

Proof: See Appendix C. ■

D. Distributed Formation Scaling Design Method

Based on the preceding analysis, the proposed online distributed formation scaling design method for the dynamics of the local scaling policy (4) and formation scaling parameter (15) can be summarized in (18), (19), and (20).

$$\mu_{i\kappa}^{\text{ref}} = -k_\kappa s_{i\kappa} - a_\kappa \ddot{\rho}_i - b_\kappa \dot{\rho}_i + k_{\kappa f} v_{i\kappa} \tag{18}$$

$$\begin{cases} \mu_{i\kappa} = \arg\min \dfrac{1}{2}\left(\mu_{i\kappa} - \mu_{i\kappa}^{\text{ref}}\right)^2 \\ s.t. \quad \xi_1 \geq 0 \\ \qquad \zeta_3 \geq 0 \end{cases} \tag{19}$$

$$\begin{aligned}
u_{i\kappa} =& \ddot{\rho}_i - a_\kappa(\dot{\kappa}_i - \dot{\rho}_i) - b_\kappa(\kappa_i - \rho_i) \\
& - \varphi_\kappa \sum_{j \in \boldsymbol{\mathcal{N}}_i} \operatorname{sgn}(\kappa_i - \kappa_j) - \pi_\kappa \sum_{j \in \boldsymbol{\mathcal{N}}_i} \operatorname{sgn}(\dot{\kappa}_i - \dot{\kappa}_j)
\end{aligned} \tag{20}$$

where the parameters satisfy $a_\kappa > 1$; b_κ, k_κ, $k_{\kappa f}$, ε_κ, γ_κ, $\delta_{1\kappa}$, $\delta_{2\kappa}$, $\delta_{3\kappa}$ are positive gains, and

$$\begin{cases} 1 = \delta_{1\kappa} + \delta_{2\kappa} + \delta_{3\kappa} - a_\kappa - 0.25\gamma_\kappa \\ a_\kappa = \delta_{2\kappa}\delta_{1\kappa} + \delta_{3\kappa}\delta_{1\kappa} + \delta_{3\kappa}\delta_{2\kappa} - b_\kappa - 0.25\gamma_\kappa a_\kappa \\ b_\kappa = \delta_{3\kappa}\delta_{2\kappa}\delta_{1\kappa} - 0.25\gamma_\kappa b_\kappa \\ \varphi_\kappa > n(n-1)\varepsilon_\kappa \\ \pi_\kappa > \varphi_\kappa + n(n-1)\varepsilon_\kappa \end{cases}. \tag{21}$$

IV. Formation Translation Parameter Design

This section describes the manner in which the formation translation parameter reach an agreement for bearing-preserving maneuvers. Unlike the local scaling policy design, the local excitation vector $\boldsymbol{f}_i$ can be exerted directly on formation translation, and the minimum constraint is unnecessary. The other steps are similar to those described in Section III for formation scaling parameter design.

A. Unconstrained Local Translation Policy Design

It is considered that the local translation policy $\boldsymbol{w}_i \in \mathbb{R}^3$ is governed by the following virtual triple-integrator system (22):

$$\dddot{\boldsymbol{w}}_i = \boldsymbol{\mu}_{iq}, \tag{22}$$

where $\boldsymbol{\mu}_{iq}$ is the input.

The unconstrained nominal control law is designed as follows:

$$\boldsymbol{\mu}_{iq} = \dddot{\boldsymbol{p}}^* - k_q \boldsymbol{s}_{iq} - a_q\left(\ddot{\boldsymbol{w}}_i - \ddot{\boldsymbol{p}}^*\right) - b_q\left(\dot{\boldsymbol{w}}_i - \dot{\boldsymbol{p}}^*\right) + k_{qf}\boldsymbol{f}_i, \tag{23}$$

where $k_q > 0$, $a_q > 1$, and $b_q > 0$; $k_{qf} > 0$ is a gain that adjusts the effect of $\boldsymbol{f}_i$. A larger k_{qf} allows the translation excitation to more easily translate the formation. s_{iq} is the sliding mode surface, which is defined as

$$\boldsymbol{s}_{iq} = \left(\ddot{\boldsymbol{w}}_i - \ddot{\boldsymbol{p}}^*\right) + a_q\left(\dot{\boldsymbol{w}}_i - \dot{\boldsymbol{p}}^*\right) + b_q\left(\boldsymbol{w}_i - \boldsymbol{p}^*\right). \tag{24}$$

Theorem 4: Under Assumption 2, with any $k_q > 0$, $a_q > 1$, $b_q > 0$, and $k_{qf} > 0$ for the dynamics (22) and control (23), if $\boldsymbol{f}_i = \boldsymbol{0}$, then $(\ddot{\boldsymbol{w}}_i, \dot{\boldsymbol{w}}_i, \boldsymbol{w}_i)$ converges to $(\boldsymbol{0}, \boldsymbol{0}, \boldsymbol{0})$. If $\boldsymbol{f}_i \neq \boldsymbol{0}$, then a local translation policy with the effect of $\boldsymbol{f}_i$ is generated.

Proof: The proof of this result is quite similar to that of Theorem 1; and hence, it is omitted. ■

B. Constrained Local Translation Policy Design

Unlike formation scaling, it is unnecessary to constrain the minimum formation translation. Note that only one constraint exists for formation translation policies:

$$h_3\left(\boldsymbol{w}_i, \dot{\boldsymbol{w}}_i, \ddot{\boldsymbol{w}}_i\right) = \varepsilon_q^2 - \left\|\boldsymbol{s}_{iq}\right\|_2^2 \geq 0, \tag{25}$$

where $\varepsilon_q > 0$ can be designed. The constraint $h_3\left(\boldsymbol{w}_i, \dot{\boldsymbol{w}}_i, \ddot{\boldsymbol{w}}_i\right) : \mathbb{R}^9 \to \mathbb{R}$ is designed for the consensus filter, as will be described in the next subsection. It requires that $\boldsymbol{w}_i$, $\dot{\boldsymbol{w}}_i$, and $\ddot{\boldsymbol{w}}_i$ are always in the forward invariant set $\mathcal{C}_q$, defined as

$$\mathcal{C}_q := \left\{ \begin{bmatrix} \boldsymbol{w}_i^{\mathrm{T}} & \dot{\boldsymbol{w}}_i^{\mathrm{T}} & \ddot{\boldsymbol{w}}_i^{\mathrm{T}} \end{bmatrix}^{\mathrm{T}} \in \mathbb{R}^9 : h_3\left(\boldsymbol{w}_i\right) \geq 0 \right\}. \tag{26}$$

We will omit arguments $\boldsymbol{w}_i$, $\dot{\boldsymbol{w}}_i$, and $\ddot{\boldsymbol{w}}_i$ when it is clear that we are referring to $h_3\left(\boldsymbol{w}_i, \dot{\boldsymbol{w}}_i, \ddot{\boldsymbol{w}}_i\right)$. We consider the following series of functions:

$$\begin{aligned}
\varsigma_0 =& h_3, \\
\varsigma_1 =& \dot{\varsigma}_0 + \gamma_p \varsigma_0 \\
=& \dot{h}_3 + \gamma_p h_3 \\
=& 2\boldsymbol{s}_{iq}^{\mathrm{T}}\left[-\dddot{\boldsymbol{p}}^* + a_q\left(\ddot{\boldsymbol{w}}_i - \ddot{\boldsymbol{p}}^*\right) + b_q\left(\dot{\boldsymbol{w}}_i - \dot{\boldsymbol{p}}^*\right)\right] \\
& 2\boldsymbol{s}_{iq}^{\mathrm{T}}\boldsymbol{\mu}_{iq} + \gamma_q\left(\varepsilon_q^2 - \left\|\boldsymbol{s}_{iq}\right\|_2^2\right),
\end{aligned}$$

where $\gamma_q \varsigma_0$ is a class $\mathcal{K}$ function with $\gamma_q > 0$.

The relative degree of h_3 with respect to system (22) is 1. The modified control $\boldsymbol{\mu}_{iq}$ from a nominal control $\boldsymbol{\mu}_{iq}^{\text{ref}}$ can be obtained by the following CBF QP:

$$\begin{cases} \boldsymbol{\mu}_{iq} = \arg\min \dfrac{1}{2}\left(\boldsymbol{\mu}_{iq} - \boldsymbol{\mu}_{iq}^{\text{ref}}\right)^2 \\ s.t. \quad \varsigma_1 \geq 0 \end{cases}. \tag{27}$$

where

$$\boldsymbol{\mu}_{iq}^{\text{ref}} = \dddot{\boldsymbol{p}}^* - k_q \boldsymbol{s}_{iq} - a_q\left(\ddot{\boldsymbol{w}}_i - \ddot{\boldsymbol{p}}^*\right) - b_q\left(\dot{\boldsymbol{w}}_i - \dot{\boldsymbol{p}}^*\right) + k_{qf}\boldsymbol{f}_i,$$

which is the unconstrained nominal control proposed in (23).

C. Distributed Translation Consensus Filter

Diverse local translation policies are generated using (22), (23), and (27). Further, a unique translation parameter should be given for bearing-preserving motions. The formation translation parameter is governed by the following dynamics:

$$\ddot{\boldsymbol{q}}_i = \boldsymbol{u}_{iq}. \tag{28}$$

A DAT-based consensus filter is presented in (29), which can integrate local translation policies in a weighted-average manner.

$$\begin{aligned}
\boldsymbol{u}_{iq} =& \ddot{\boldsymbol{w}}_i - a_q\left(\dot{\boldsymbol{q}}_i - \dot{\boldsymbol{w}}_i\right) - b_q\left(\boldsymbol{q}_i - \boldsymbol{w}_i\right) \\
& - \varphi_q \sum_{j \in \mathcal{N}_i} \operatorname{sgn}\left(\boldsymbol{q}_i - \boldsymbol{q}_j\right) - \pi_q \sum_{j \in \mathcal{N}_i} \operatorname{sgn}\left(\dot{\boldsymbol{q}}_i - \dot{\boldsymbol{q}}_j\right),
\end{aligned} \tag{29}$$

where the following conditions should be satisfied:

$$\begin{cases} \varphi_q > n\left(n-1\right)\varepsilon_q \\ \pi_q > \varphi_q + n\left(n-1\right)\varepsilon_q \end{cases}. \tag{30}$$

Theorem 5: Under Assumption 1, if (30) is satisfied, then the DAT-based consensus filter (29) can enforce formation translation parameters with dynamics (28) to reach a consensus, which is exactly the weighted average of local translation policies.

Proof: The proof of this result is quite similar to that of Theorem 3; and hence, it is omitted. ■

D. Distributed Formation Translation Design Method

Based on the preceding analysis, the proposed online distributed formation translation design method for local translation dynamics (22) and formation translation parameter dynamics (28) can be summarized in (31), (32), and (33).

$$\boldsymbol{\mu}_{iq}^{\text{ref}} = \dddot{\boldsymbol{p}}^* - k_q \boldsymbol{s}_{iq} - a_q\left(\ddot{\boldsymbol{w}}_i - \ddot{\boldsymbol{p}}^*\right) - b_q\left(\dot{\boldsymbol{w}}_i - \dot{\boldsymbol{p}}^*\right) + k_{qf}\boldsymbol{f}_i, \tag{31}$$

$$\begin{cases} \boldsymbol{\mu}_{iq} = \arg\min \dfrac{1}{2}\left(\boldsymbol{\mu}_{iq} - \boldsymbol{\mu}_{iq}^{\text{ref}}\right)^2 \\ s.t. \quad \varsigma_1\left(\boldsymbol{w}_i\right) \geq 0 \end{cases}, \tag{32}$$

$$\begin{aligned}
\boldsymbol{u}_{iq} =& \ddot{\boldsymbol{w}}_i - a_q\left(\dot{\boldsymbol{q}}_i - \dot{\boldsymbol{w}}_i\right) - b_q\left(\boldsymbol{q}_i - \boldsymbol{w}_i\right) \\
& - \varphi_q \sum_{j \in \mathcal{N}_i} \operatorname{sgn}\left(\boldsymbol{q}_i - \boldsymbol{q}_j\right) - \pi_q \sum_{j \in \mathcal{N}_i} \operatorname{sgn}\left(\dot{\boldsymbol{q}}_i - \dot{\boldsymbol{q}}_j\right),
\end{aligned} \tag{33}$$

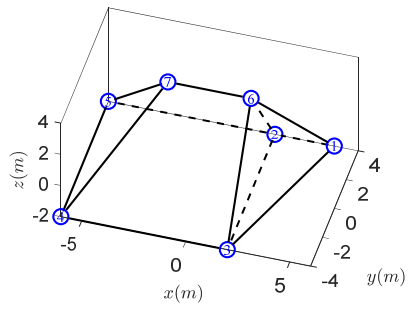

$$\begin{aligned}
\boldsymbol{r}_1^* &= [\ 6 \quad 0 \quad 2]^T \\
\boldsymbol{r}_2^* &= [\ 2 \quad 4 \quad -2]^T \\
\boldsymbol{r}_3^* &= [\ 2 \quad -4 \quad -2]^T \\
\boldsymbol{r}_4^* &= [-6 \quad -4 \quad -2]^T \\
\boldsymbol{r}_5^* &= [-6 \quad 4 \quad -2]^T \\
\boldsymbol{r}_6^* &= [\ 2 \quad 4 \quad 4]^T \\
\boldsymbol{r}_7^* &= [-2 \quad 0 \quad 4]^T
\end{aligned}$$

Fig. 4. The nominal formation and communication topologies in simulation.

where the parameters satisfy $a_q > 1$; b_q, k_q, k_{qf}, ε_p, γ_q are positive gains, and

$$\begin{cases} \varphi_q > n\,(n-1)\,\varepsilon_q \\ \pi_q > \varphi_q + n\,(n-1)\,\varepsilon_q \end{cases}. \tag{34}$$

Remark 2: By designing the local excitation vector $\boldsymbol{f}_i$, collective behaviors such as obstacle avoidance and containment can be obtained. When dealing with static obstacles, the local excitation $\boldsymbol{f}_i$ can be generated based on the relative position of the obstacles and the robots. However, in the case of dynamic obstacles, their velocities must be considered when designing the local excitation vector $\boldsymbol{f}_i$. Specifically, when an obstacle is approaching the robot, a larger excitation should be generated to enable the robot to maneuver quickly and avoid the obstacle. On the contrary, when the obstacle is moving away from the robot, the avoidance requirement needs not be considered immediately, and a smaller excitation is sufficient.

V. Simulation and Experiment Results

This section discusses the numerical simulations and experiments conducted to validate the theoretical results of the proposed online distributed dynamic formation design method. A classic distributed formation control [10] is utilized for the generated desired position $\boldsymbol{p}_i^d = \boldsymbol{q}_i + \kappa_i \boldsymbol{r}_i^*$ tracking, where the parameters $\boldsymbol{q}_i$ and κ_i are obtained using the proposed formation variation parameter design methods summarized in Section III-D and IV-D.

A. Simulation

Seven robots are considered in an environment with obstacles. The nominal formation and communication topologies are illustrated in Fig. 4. The initial formation scale and translation are set to the nominal formation, such that

$$\begin{aligned}
\kappa_i\,(0) = \rho_i\,(0) = \kappa^* = 1, \\
\boldsymbol{w}_i\,(0) = \boldsymbol{q}_i\,(0) = \boldsymbol{0}, \\
\boldsymbol{p}_i\,(0) = \boldsymbol{p}_i^d\,(0)\,.
\end{aligned}$$

The parameters for the formation scaling design are selected as

$$\begin{cases} \delta_{1\kappa} = 1.5 \\ \delta_{2\kappa} = 1.2576 \\ \delta_{3\kappa} = 1.25 \\ \gamma_\kappa = 1 \end{cases} \begin{cases} a_\kappa = 2.7576 \\ b_\kappa = 1.8863 \\ k_\kappa = 10 \\ k_{\kappa f} = 70 \end{cases} \begin{cases} \varphi_\kappa = 100 \\ \pi_\kappa = 200 \\ \varepsilon_\kappa = 1.5 \\ \kappa_{\min} = 0.3 \end{cases},$$

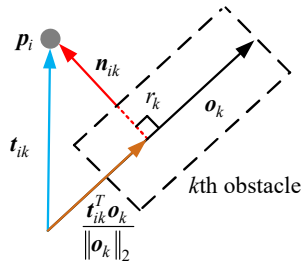

Fig. 5. The computation of $\bar{\boldsymbol{n}}_{ik}$ in simulation. $\boldsymbol{o}_k$ is the axis of kth cylinder obstacle. $\boldsymbol{t}_{ik}$ is a vector from any point on $\boldsymbol{o}_k$ to the robot $\boldsymbol{p}_i$. $\boldsymbol{n}_{ik} = \boldsymbol{t}_{ik} - \frac{\boldsymbol{t}_{ik}^{\mathrm{T}} \boldsymbol{o}_k}{\|\boldsymbol{o}_k\|_2}$. Thereby, $\bar{\boldsymbol{n}}_{ik} = \frac{\|\boldsymbol{n}_{ik}\|_2 - r_k}{\|\boldsymbol{n}_{ik}\|_2^2} \boldsymbol{n}_{ik}$ is obtained.

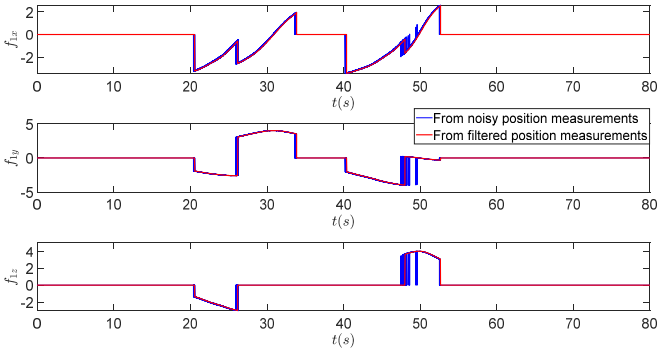

Fig. 6. The computed $\boldsymbol{f}_1$ from noisy and filtered position measurements in simulation.

which satisfies Theorems 1, 2, and 3. The parameters for the formation translation design are selected as

$$\begin{cases} k_q = 10 \\ k_{qf} = 70 \end{cases} \begin{cases} a_q = 2.8363 \\ b_q = 2.0111 \\ \gamma_q = 1 \end{cases} \begin{cases} \varphi_q = 300 \\ \pi_q = 600\,, \\ \varepsilon_q = 7 \end{cases}$$

which satisfies Theorems 4 and 5.

Obstacles are modeled as cylinders. The kth cylinder has axis $\boldsymbol{o}_k$ and radius r_k. The local excitation vector $\boldsymbol{f}_i$ is generated using the following simple rules:

$$\boldsymbol{f}_i = \begin{cases} 4\dfrac{\bar{\boldsymbol{n}}_{i,\min}}{\|\bar{\boldsymbol{n}}_{i,\min}\|_2} & \|\bar{\boldsymbol{n}}_{i,\min}\|_2 \le 5 \\ 0 & \|\bar{\boldsymbol{n}}_{i,\min}\|_2 > 5 \end{cases}, \tag{35}$$

where $\bar{\boldsymbol{n}}_{i,\min} = \min\{\bar{\boldsymbol{n}}_{ik}\}$. $\bar{\boldsymbol{n}}_{ik}$ denotes the vector from the nearest point of the kth obstacle surface to the ith robot. The computation of $\bar{\boldsymbol{n}}_{ik}$ is shown in Fig. 5. The rules in (35) imply that $\boldsymbol{f}_i$ is activated only by the nearest obstacle. Note that $\boldsymbol{f}_i$ can be discontinuous.

In the practical system, $\boldsymbol{f}_i$ can be disturbed by noisy position measurements. Therefore, in the simulation, to simulate the practical environment, Gaussian noise is considered in robots' position measurements. The noisy measurements are processed using low-pass filters, which have been widely used to handle the measurement noises [43]-[44]. Fig. 6 shows the computed $\boldsymbol{f}_1$ from noisy and filtered position measurements, respectively. The noisy $\boldsymbol{f}_1$ has more chattering because the noise causes frequent switching of the $\min\{\cdot\}$ function in (35). The filtered

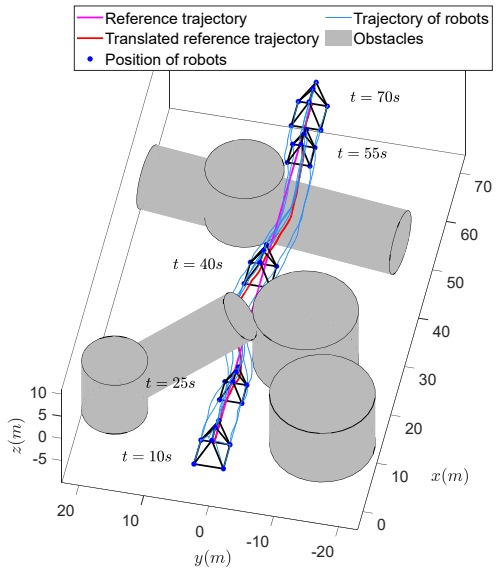

Fig. 7. The formation variations in simulation.

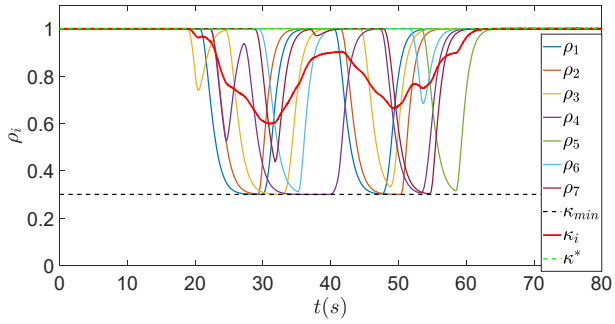

Fig. 8. Local scaling policies and formation scaling parameters in simulation.

$\boldsymbol{f}_1$ does not have chattering, and it can be observed that the low-pass filters can handle the measurement noise effectively.

The variations in formation are shown in Fig. 7. The reference trajectory, denoted by the straight pink line, is close to the obstacles in some areas. With the help of the excitation vector $\boldsymbol{f}_i$ and the proposed dynamic formation maneuver methods, a uniform translated reference trajectory and scaled formation are obtained. This result indicates that the robots are adaptive to an environment with obstacles under bearing constraints.

According to $\boldsymbol{f}_i$, diverse local scaling and translation policies are generated, as shown in Fig. 8 and Fig. 9, respectively, where the consensus filters resulting in a uniform formation scale and translation are highlighted in red.

The performance of the constraints $h_1 > 0$, $h_2 > 0$, and $h_3 > 0$ is shown in Fig. 10, Fig. 8 and Fig. 11, respectively. It is observed that the designed constraints of the local variation policies are well satisfied under the proposed CBFs.

B. Experiment

Fig. 12 presents the framework of the physical experiment system. The aerial robots utilized are Crazyflies[1]. The position

[1]https://www.bitcraze.io/products/crazyflie-2-1/

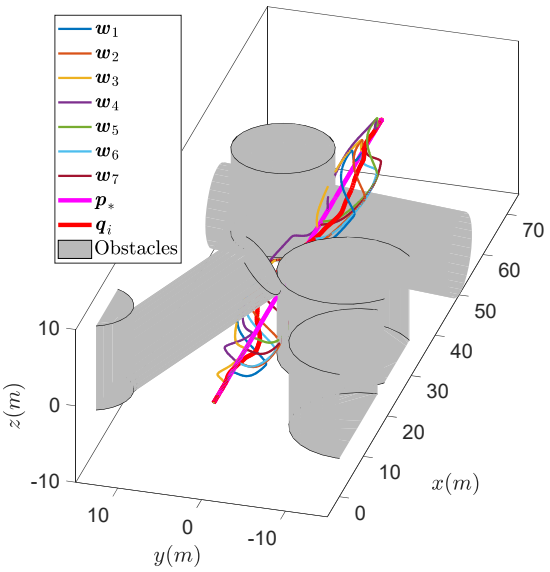

Fig. 9. Local translation policies and formation translation parameters in simulation.

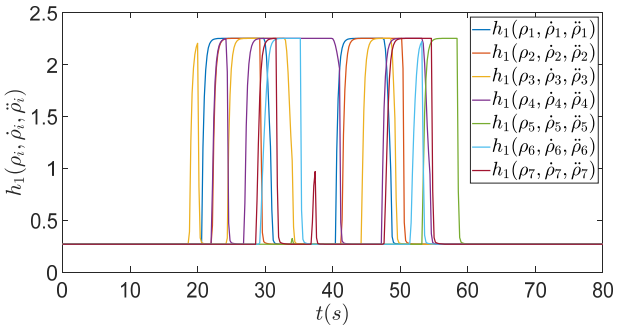

Fig. 10. Constraint $h_1 > 0$ in simulation.

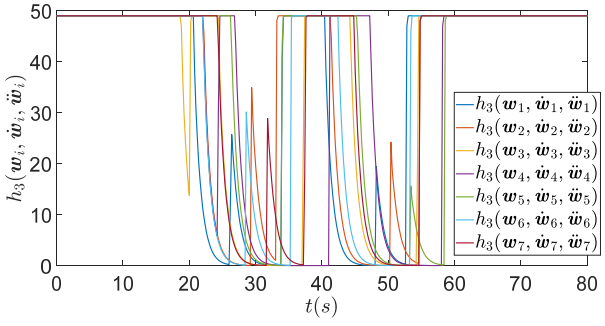

Fig. 11. Constraint $h_3 > 0$ in simulation.

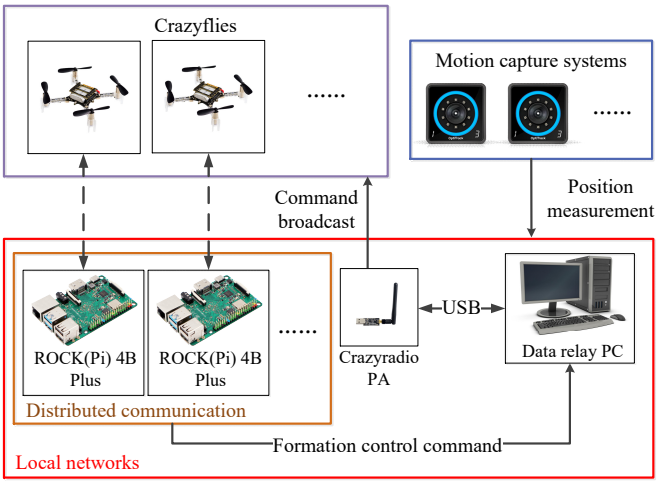

Fig. 12. The framework of experiment system and data flow.

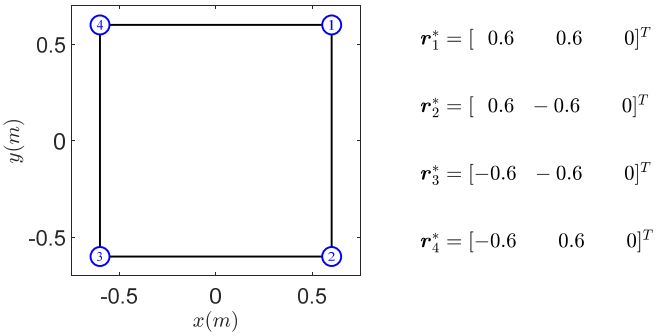

$$\boldsymbol{r}_1^* = [\ 0.6 \quad 0.6 \quad 0]^T$$
$$\boldsymbol{r}_2^* = [\ 0.6 \quad -0.6 \quad 0]^T$$
$$\boldsymbol{r}_3^* = [-0.6 \quad -0.6 \quad 0]^T$$
$$\boldsymbol{r}_4^* = [-0.6 \quad 0.6 \quad 0]^T$$

Fig. 13. The nominal formation and communication topologies in the experiment.

measurements are supported by OptiTrack[2] motion capture systems. The proposed distributed formation scaling and translation parameter design methods are deployed on ROCK(Pi) 4B Plus[3] onboard processors, each of which corresponds to a single Crazyflie. The control commands are broadcast through a data relay PC using the Crazyradio PA[4] data transmission module.

Four Crazyflies are considered in a planar obstacle environment. The nominal formation and communication topologies are illustrated in Fig.13. The initial formation scale and translation are set to the nominal formation, such that

$$\kappa_i(0) = \rho_i(0) = \kappa^* = 1,$$

$$\boldsymbol{w}_i(0) = \boldsymbol{q}_i(0) = \boldsymbol{0},$$

$$\boldsymbol{p}_i(0) = \boldsymbol{p}_i^d(0).$$

[2]https://www.optitrack.com/
[3]https://wiki.radxa.com/Rockpi4
[4]https://www.bitcraze.io/products/crazyradio-pa/

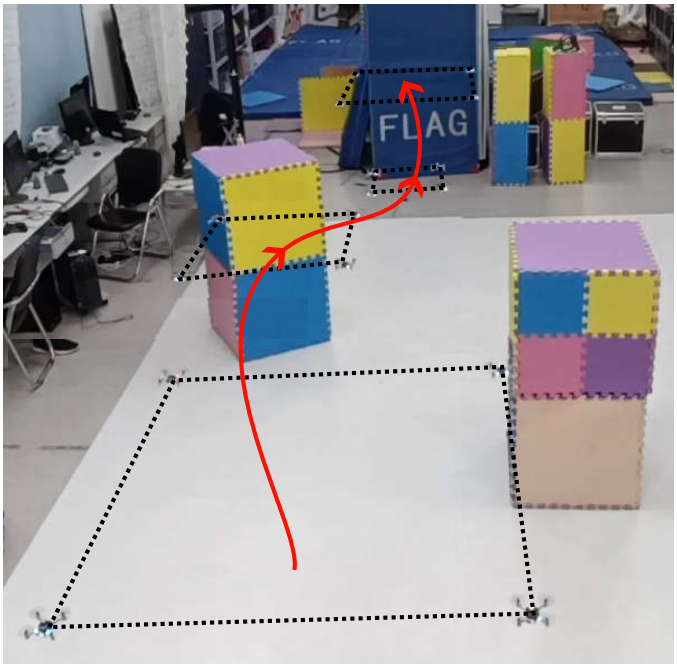

Fig. 14. Snapshots of the experiment.

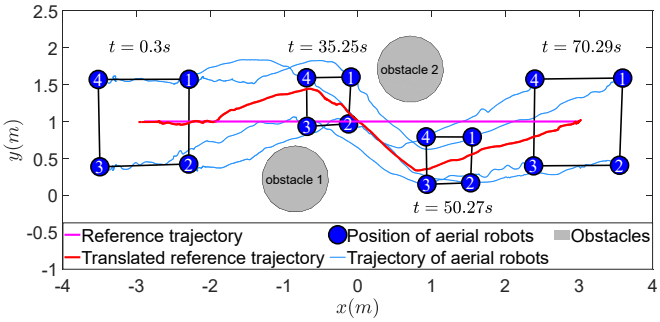

Fig. 15. The formation variations in the experiment.

The parameters for the formation scaling design are selected as

$$\begin{cases} \delta_{1\kappa} = 1.5 \\ \delta_{2\kappa} = 1.2576 \\ \delta_{3\kappa} = 1.25 \\ \gamma_\kappa = 1 \end{cases} \begin{cases} a_\kappa = 2.7576 \\ b_\kappa = 1.8863 \\ k_\kappa = 10 \\ k_{\kappa f} = 100 \end{cases} \begin{cases} \varphi_\kappa = 20 \\ \pi_\kappa = 40 \\ \varepsilon_\kappa = 1.5 \\ \kappa_{\min} = 0.3 \end{cases},$$

which satisfies Theorems 1, 2, and 3. The parameters for the formation translation design are selected as

$$\begin{cases} k_q = 10 \\ k_{qf} = 5 \end{cases} \begin{cases} a_q = 2.8363 \\ b_q = 2.0111 \\ \gamma_q = 1 \end{cases} \begin{cases} \varphi_q = 45 \\ \pi_q = 90 \\ \varepsilon_q = 3.5 \end{cases},$$

which satisfies Theorems 4 and 5.

Two obstacles are modeled as planar circles with the same radius 0.45 m. The excitation vector $\boldsymbol{f}_i$ is generated using the artificial potential fields from the obstacles.

As shown in Fig. 14 and Fig. 15, four aerial robots with a square formation move along the obtained translated reference

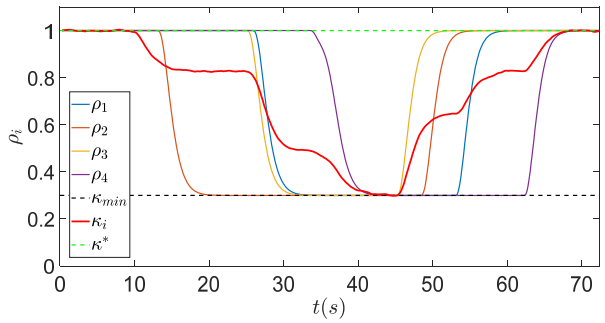

Fig. 16. Local scaling policies and formation scaling parameters in the experiment.

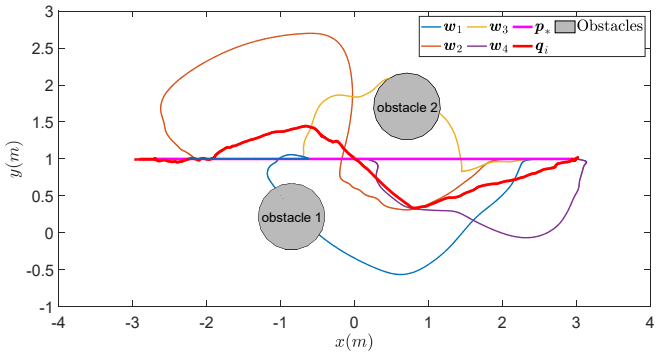

Fig. 17. Local translation policies and formation translation parameters in the experiment.

trajectory in an environment with obstacles. The formation scale is also automatically transformed.

Owing to the effect of the excitation vector $\boldsymbol{f}_i$, diverse local scaling and translation policies are generated, as shown in Fig. 16 and Fig. 17, respectively. The team of robots follows the designed uniform translation parameters $\boldsymbol{q}_i$, which are shown in red in Fig. 15 and Fig. 17. From Fig. 17, it is observed that the generated local translation trajectories of robots 1 and 3 cross the obstacles, but no collisions occur because the generated local variation policies $\boldsymbol{w}_i$ are responsible only for themselves. $\boldsymbol{q}_i$ is the integration of the local variation policies $\{\boldsymbol{w}_i\}_{i=1}^n$. Hence, if one robot wants to affect the whole significantly, it must be significantly "loud." For example, as illustrated in Fig. 15, robot 1 is always close to obstacle 2, located at $\begin{bmatrix}0.71 & 1.71\end{bmatrix}^{\mathrm{T}}$. Although its neighboring robots 2 and 4 can also be affected by obstacle 2 , the distance from obstacle 2 to these robots is still large. The generated $\boldsymbol{w}_2$ and $\boldsymbol{w}_4$ are only slightly affected by obstacle 2. Hence, the consequent translation parameter drives robot 1 to continue approaching obstacle 2, and the magnitude of $\boldsymbol{f}_1$ continues to increase until $\boldsymbol{w}_1$ becomes significantly distant from obstacle 2. At this time, $\boldsymbol{w}_1$ can cross obstacles far from robot 1.

The performance of constraints $h_1 > 0$, $h_2 > 0$, and $h_3 > 0$ is shown in Fig. 18, Fig. 16 and Fig. 19, respectively. It is observed that the designed constraints of the local policies are well satisfied.

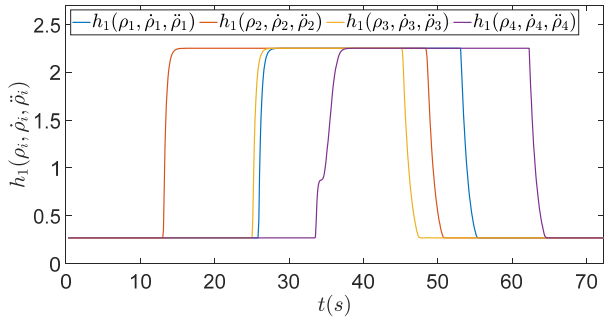

Fig. 18. Constraint $h_1 > 0$ in the experiment.

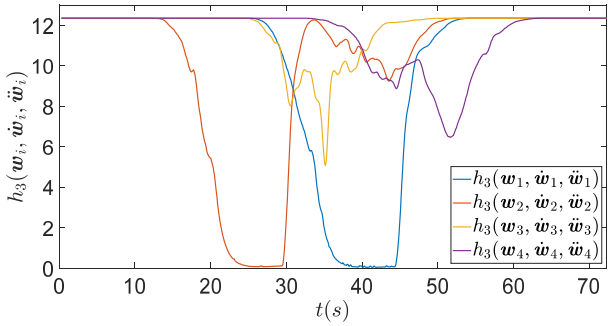

Fig. 19. Constraint $h_3 > 0$ in the experiment.

VI. Conclusion

This paper has proposed an online distributed formation design method for scaling and translation parameters that can maintain bearing constraints in dynamic formation maneuvers. The formation motions were excited by time-varying discontinuous environmental excitation vectors $\boldsymbol{f}_i$. By using HOCBF-based control, continuous bounded local variation policies were generated for DAT algorithms, obtaining uniform formation variation parameters, which are exactly the weighted average of local variation policies. Based on simulations with up to seven robots and experiments with up to four robots, we demonstrated successful dynamic formation maneuvers. The robots could scale and translate the entire formation when required in response to the environment.

Future research will include extending the proposed design methods to more types of formation variations and more complex constraints.

Appendix

A. *Proof of Theorem 1*

According to (6) and (7), it has

$$\begin{aligned}\dot{s}_{i\kappa} &= \dddot{\rho}_i + a_\kappa \ddot{\rho}_i + b_\kappa \dot{\rho}_i \\ &= -k_\kappa s_{i\kappa} + k_{\kappa f} v_{i\kappa}.\end{aligned}$$

Then, we select the Lyapunov function $V_{s_{i\kappa}} = \frac{1}{2} s_{i\kappa}^2$, whose derivative is

$$\begin{aligned}\dot{V}_{s_{i\kappa}} =& s_{i\kappa}\dot{s}_{i\kappa} \\ =& -k_\kappa s_{i\kappa}^2 + k_{\kappa f} s_{i\kappa} v_{i\kappa}.\end{aligned}$$

According to Assumption 2, $v_{i\kappa}$ is finite. When $v_{i\kappa} \neq 0$, $s_{i\kappa}$ can converge to the neighborhood of 0, represented by $s_{i\kappa} = \eta_{i\kappa}(v_{i\kappa})$, where $\eta_{i\kappa}(v_{i\kappa})$ is finite. By substituting $s_{i\kappa} = \eta_{i\kappa}(v_{i\kappa})$ into (7), the motion of ρ_i is obtained by

$$\ddot{\rho}_i = -a_\kappa \dot{\rho}_i - b_\kappa(\rho_i - \kappa^*) + \eta_{i\kappa}(v_{i\kappa}).$$

A Lyapunov function is selected as

$$V_{\rho_i} = \frac{1}{2}\begin{bmatrix}(\rho_i - \kappa^*)\\ \dot{\rho}\end{bmatrix}^{\mathrm{T}}\begin{bmatrix}a_\kappa + b_\kappa & 1\\ 1 & 1\end{bmatrix}\begin{bmatrix}(\rho_i - \kappa^*)\\ \dot{\rho}\end{bmatrix},$$

whose derivative is

$$\begin{aligned}\dot{V}_{\rho_i} =& (a_\kappa + b_\kappa)(\rho_i - \kappa^*)\dot{\rho}_i + \dot{\rho}_i^2 + [(\rho_i - \kappa^*) + \dot{\rho}_i]\ddot{\rho}_i\\ =& -(a_\kappa - 1)\dot{\rho}_i^2 - b_\kappa(\rho_i - \kappa^*)^2\\ &+ [(\rho_i - \kappa^*) + \dot{\rho}_i]\eta_{i\kappa}(v_{i\kappa})\\ =& -\begin{bmatrix}(\rho_i - \kappa^*)\\ \dot{\rho}\end{bmatrix}^{\mathrm{T}}\begin{bmatrix}b_\kappa & 0\\ 0 & a_\kappa - 1\end{bmatrix}\begin{bmatrix}(\rho_i - \kappa^*)\\ \dot{\rho}\end{bmatrix}\\ &+ [(\rho_i - \kappa^*) + \dot{\rho}_i]\eta_{i\kappa}(v_{i\kappa})\\ \leq& -C_\kappa V_{\rho_i} + [(\rho_i - \kappa^*) + \dot{\rho}_i]\eta_{i\kappa}(v_{i\kappa}),\end{aligned}$$

where

$$C_\kappa = \frac{\min\{a_\kappa - 1, b_\kappa\}}{\lambda_{\max}\left(\begin{bmatrix}a_\kappa + b_\kappa & 1\\ 1 & 1\end{bmatrix}\right)}.$$

It shows that $(\ddot{\rho}_i, \dot{\rho}_i, \rho_i)$ converges to the neighborhood of $(0, 0, \kappa^*)$, which means diverse local scaling policies $\{\rho_i\}_{i=1}^n$ are generated.

If $v_{i\kappa} = 0$, it has $\dot{V}_{s_{i_\kappa}} = -k_\kappa s_{i\kappa}^2$. The sliding mode surface $s_{i\kappa} = \eta_{i\kappa}(v_{i\kappa}) = 0$ can be achieved. Then, according to $\dot{V}_{\rho_i} \leq -C_\kappa V_{\rho_i}$, $(\ddot{\rho}_i, \dot{\rho}_i, \rho_i)$ returns to $(0, 0, \kappa^*)$.

B. Proof of Theorem 2

According to

$$\begin{cases}\xi_1 \geq 0\\ \zeta_3 \geq 0\end{cases},$$

the control $\mu_{i\kappa}$ must satisfy

$$\begin{cases}P_i(\rho_i, \dot{\rho}_i, \ddot{\rho}_i) \geq Q_i(\rho_i, \dot{\rho}_i, \ddot{\rho}_i)\mu_{i\kappa}\\ \mu_{i\kappa} \geq W_i(\rho_i)\end{cases}, \tag{36}$$

where

$$Q_i(\rho_i, \dot{\rho}_i, \ddot{\rho}_i) = 2[\ddot{\rho}_i + a_\kappa\dot{\rho}_i + b_\kappa(\rho_i - \kappa_{\min})],$$

$$\begin{aligned}&P_i(\rho_i, \dot{\rho}_i, \ddot{\rho}_i)\\ =& -2[\ddot{\rho}_i + a_\kappa\dot{\rho}_i + b_\kappa(\rho_i - \kappa_{\min})](a_\kappa\ddot{\rho}_i + b_\kappa\dot{\rho}_i)\\ &+ \gamma_\kappa\left\{\varepsilon_\kappa^2 - [\ddot{\rho}_i + a_\kappa\dot{\rho}_i + b_\kappa(\rho_i - \kappa_{\min})]^2\right\}\\ =& -Q_i(\rho_i)(a_\kappa\ddot{\rho}_i + b_\kappa\dot{\rho}_i) + \gamma_\kappa\left(\varepsilon_\kappa^2 - \frac{1}{4}Q_i^2(\rho_i)\right),\end{aligned}$$

$$\begin{aligned}W_i(\rho_i) =& -(\delta_{1\kappa} + \delta_{2\kappa} + \delta_{3\kappa})\ddot{\rho}_i\\ &-(\delta_{2\kappa}\delta_{1\kappa} + \delta_{3\kappa}\delta_{1\kappa} + \delta_{3\kappa}\delta_{2\kappa})\dot{\rho}_i\\ &-\delta_{3\kappa}\delta_{2\kappa}\delta_{1\kappa}(\rho_i - \kappa_{\min}).\end{aligned}$$

We will omit arguments ρ_i, $\dot{\rho}_i$,and $\ddot{\rho}_i$ when it is clear that we are referring to $P_i(\rho_i, \dot{\rho}_i, \ddot{\rho}_i)$, $Q_i(\rho_i, \dot{\rho}_i, \ddot{\rho}_i)$, and $W_i(\rho_i)$. There are three cases according to the value of Q_i.

Case I, if $Q_i > 0$, $\mu_{i\kappa}$ can be solved from (36) as

$$\frac{P_i}{Q_i} \geq \mu_{i\kappa} \geq W_i.$$

It is considered the term:

$$\begin{aligned}&P_i - Q_iW_i\\ =& -Q_i(a_\kappa\ddot{\rho}_i + b_\kappa\dot{\rho}_i) + \gamma_\kappa\left(\varepsilon_\kappa^2 - \frac{1}{4}Q_i^2\right)\\ &+ Q_i\begin{bmatrix}(\delta_{1\kappa} + \delta_{2\kappa} + \delta_{3\kappa})\ddot{\rho}_i\\ +(\delta_{2\kappa}\delta_{1\kappa} + \delta_{3\kappa}\delta_{1\kappa} + \delta_{3\kappa}\delta_{2\kappa})\dot{\rho}_i\\ +\delta_{3\kappa}\delta_{2\kappa}\delta_{1\kappa}(\rho_i - \kappa_{\min})\end{bmatrix}\\ =& Q_i\begin{bmatrix}(\delta_{1\kappa} + \delta_{2\kappa} + \delta_{3\kappa} - a_\kappa - 0.25\gamma_\kappa)\ddot{\rho}_i\\ +(\delta_{2\kappa}\delta_{1\kappa} + \delta_{3\kappa}\delta_{1\kappa} + \delta_{3\kappa}\delta_{2\kappa} - b_\kappa - 0.25\gamma_\kappa a_\kappa)\dot{\rho}_i\\ +(\delta_{3\kappa}\delta_{2\kappa}\delta_{1\kappa} - 0.25\gamma_\kappa b_\kappa)(\rho_i - \kappa_{\min})\end{bmatrix}\\ &+ \gamma_\kappa\varepsilon_\kappa^2.\end{aligned}$$

Combining (14), it has

$$P_i - Q_iW_i = \frac{1}{2}Q_i^2 + \gamma_\kappa\varepsilon_\kappa^2 > 0,$$

which means (36) is not contradictory for $\mu_{i\kappa}$. Feasible control $\mu_{i\kappa}$ exists.

Case II, if $Q_i < 0$, (36) is rewritten as

$$\mu_{i\kappa} \geq \max\left\{W_i, \frac{P_i}{Q_i}\right\}.$$

Case III, if $Q_i = 0$, (36) is rewritten as

$$\mu_{i\kappa} \geq W_i.$$

Hence, for any $Q_i \in \mathbb{R}^n$, the feasible control $\mu_{i\kappa}$ in (13) for the dynamics (4) always exist as long as the condition (14) is satisfied.

C. Proof of Theorem 3

The control goal is to enforce formation scaling parameters to reach the average consensus of the local scaling policies, such that

$$\lim_{t\to\infty}\left|\kappa_i - \frac{1}{n}\sum_{j=1}^n\rho_j\right| \to 0, \quad \lim_{t\to\infty}\left|\dot{\kappa}_i - \frac{1}{n}\sum_{j=1}^n\dot{\rho}_j\right| \to 0.$$

The consensus error is defined as

$$\begin{aligned}\tilde{\kappa}_i &= \kappa_i - \frac{1}{n}\sum_{j=1}^n\kappa_j,\\ \dot{\tilde{\kappa}}_i &= \dot{\kappa}_i - \frac{1}{n}\sum_{j=1}^n\dot{\kappa}_j.\end{aligned}$$

They can be rewritten into the matrix form, such that

$$\begin{aligned}\tilde{\boldsymbol{\kappa}} &= \mathbf{M}\boldsymbol{\kappa},\\ \dot{\tilde{\boldsymbol{\kappa}}} &= \mathbf{M}\dot{\boldsymbol{\kappa}},\end{aligned}$$

where

$$\mathbf{M} = \mathbf{I}_n - \frac{1}{n}\boldsymbol{I}_n^{\mathrm{T}}\boldsymbol{I}_n,$$
$$\boldsymbol{\kappa} = \begin{bmatrix}\kappa_1 & \cdots & \kappa_n\end{bmatrix}^{\mathrm{T}},$$

and it can be verified that

$$\mathbf{M}\boldsymbol{\mathcal{H}} = \boldsymbol{\mathcal{H}},$$
$$\mathbf{M}\boldsymbol{\mathcal{L}} = \boldsymbol{\mathcal{L}}\mathbf{M} = \boldsymbol{\mathcal{L}}.$$

Then, we have

$$\begin{aligned}\ddot{\tilde{\boldsymbol{\kappa}}} =& \mathbf{M}\ddot{\boldsymbol{\kappa}}\\ =& \mathbf{M}\ddot{\boldsymbol{\rho}} - (\alpha\dot{\tilde{\boldsymbol{\kappa}}} + \beta\tilde{\boldsymbol{\kappa}}) + \mathbf{M}(a_\kappa\dot{\boldsymbol{\rho}} + b_\kappa\boldsymbol{\rho})\\ &- \varphi_\kappa\boldsymbol{\mathcal{H}}\mathrm{sgn}(\boldsymbol{\mathcal{H}}^{\mathrm{T}}\dot{\tilde{\boldsymbol{\kappa}}}) - \pi_\kappa\boldsymbol{\mathcal{H}}\mathrm{sgn}(\boldsymbol{\mathcal{H}}^{\mathrm{T}}\tilde{\boldsymbol{\kappa}}).\end{aligned}$$

We choose the following Lyapunov function:

$$\begin{aligned}V_\kappa =& \frac{1}{2}\begin{bmatrix}\tilde{\boldsymbol{\kappa}}\\ \dot{\tilde{\boldsymbol{\kappa}}}\end{bmatrix}^{\mathrm{T}}\left(\begin{bmatrix}\alpha+\beta & 1\\ 1 & 1\end{bmatrix}\right)\begin{bmatrix}\tilde{\boldsymbol{\kappa}}\\ \dot{\tilde{\boldsymbol{\kappa}}}\end{bmatrix}\\ &+ \pi_\kappa\sum_{i=1}^{n}\sum_{j\in\boldsymbol{\mathcal{N}}_i}\int_0^{\tilde{\kappa}_i-\tilde{\kappa}_j}\mathrm{sgn}\,(s)ds.\end{aligned}$$

According to $a_\kappa > 1$, $b_\kappa > 0$, it is known $V_\kappa > 0$. The derivative of V_κ is

$$\begin{aligned}\dot{V}_\kappa =& (a_\kappa + b_\kappa)\,\tilde{\boldsymbol{\kappa}}^{\mathrm{T}}\dot{\tilde{\boldsymbol{\kappa}}} + \dot{\tilde{\boldsymbol{\kappa}}}^{\mathrm{T}}\dot{\tilde{\boldsymbol{\kappa}}} + \left(\tilde{\boldsymbol{\kappa}}^{\mathrm{T}} + \dot{\tilde{\boldsymbol{\kappa}}}^{\mathrm{T}}\right)\ddot{\tilde{\boldsymbol{\kappa}}}\\ &+ \pi_\kappa\sum_{i=1}^{n}\sum_{j\in\boldsymbol{\mathcal{N}}_i}\left(\dot{\tilde{\kappa}}_i - \dot{\tilde{\kappa}}_j\right)\mathrm{sgn}\,(\tilde{\kappa}_i - \tilde{\kappa}_j)\\ =& (a_\kappa + b_\kappa)\,\tilde{\boldsymbol{\kappa}}^{\mathrm{T}}\dot{\tilde{\boldsymbol{\kappa}}} + \dot{\tilde{\boldsymbol{\kappa}}}^{\mathrm{T}}\dot{\tilde{\boldsymbol{\kappa}}} - \left(\tilde{\boldsymbol{\kappa}}^{\mathrm{T}} + \dot{\tilde{\boldsymbol{\kappa}}}^{\mathrm{T}}\right)\left(a_\kappa\dot{\tilde{\boldsymbol{\kappa}}} + b_\kappa\tilde{\boldsymbol{\kappa}}\right)\\ &+ \left(\tilde{\boldsymbol{\kappa}}^{\mathrm{T}} + \dot{\tilde{\boldsymbol{\kappa}}}^{\mathrm{T}}\right)\mathbf{M}(\ddot{\boldsymbol{\rho}} + a_\kappa\dot{\boldsymbol{\rho}} + b_\kappa\boldsymbol{\rho})\\ &- \varphi_\kappa\left(\tilde{\boldsymbol{\kappa}}^{\mathrm{T}} + \dot{\tilde{\boldsymbol{\kappa}}}^{\mathrm{T}}\right)\boldsymbol{\mathcal{H}}\mathrm{sgn}(\boldsymbol{\mathcal{H}}^{\mathrm{T}}\dot{\tilde{\boldsymbol{\kappa}}})\\ &- \pi_\kappa\left(\tilde{\boldsymbol{\kappa}}^{\mathrm{T}} + \dot{\tilde{\boldsymbol{\kappa}}}^{\mathrm{T}}\right)\boldsymbol{\mathcal{H}}\mathrm{sgn}(\boldsymbol{\mathcal{H}}^{\mathrm{T}}\tilde{\boldsymbol{\kappa}}) + \pi_\kappa\dot{\tilde{\boldsymbol{\kappa}}}^{\mathrm{T}}\boldsymbol{\mathcal{H}}\mathrm{sgn}(\boldsymbol{\mathcal{H}}^{\mathrm{T}}\tilde{\boldsymbol{\kappa}})\\ =& -(a_\kappa - 1)\dot{\tilde{\boldsymbol{\kappa}}}^{\mathrm{T}}\dot{\tilde{\boldsymbol{\kappa}}} - b_\kappa\tilde{\boldsymbol{\kappa}}^{\mathrm{T}}\tilde{\boldsymbol{\kappa}} + \left(\tilde{\boldsymbol{\kappa}}^{\mathrm{T}} + \dot{\tilde{\boldsymbol{\kappa}}}^{\mathrm{T}}\right)\mathbf{M}\boldsymbol{\chi}\\ &- \varphi_\kappa\tilde{\boldsymbol{\kappa}}^{\mathrm{T}}\boldsymbol{\mathcal{H}}\mathrm{sgn}(\boldsymbol{\mathcal{H}}^{\mathrm{T}}\dot{\tilde{\boldsymbol{\kappa}}}) - \varphi_\kappa\dot{\tilde{\boldsymbol{\kappa}}}^{\mathrm{T}}\boldsymbol{\mathcal{H}}\mathrm{sgn}(\boldsymbol{\mathcal{H}}^{\mathrm{T}}\dot{\tilde{\boldsymbol{\kappa}}})\\ &- \pi_\kappa\tilde{\boldsymbol{\kappa}}^{\mathrm{T}}\boldsymbol{\mathcal{H}}\mathrm{sgn}(\boldsymbol{\mathcal{H}}^{\mathrm{T}}\tilde{\boldsymbol{\kappa}})\end{aligned}$$

where $\chi_i = \ddot{\rho}_i + a_\kappa\dot{\rho}_i + b_\kappa\rho_i$, and

$$\boldsymbol{\chi} = \begin{bmatrix}\chi_1 & \cdots & \chi_n\end{bmatrix}^{\mathrm{T}}.$$

(13) can constraint the local scaling policies satisfy (8). Hence, we know that

$$|\ddot{\rho}_i + a_\kappa\dot{\rho}_i + b_\kappa\left(\rho_i - \kappa_{\min}\right)| \le \varepsilon_\kappa,$$

$$|\chi_i - \chi_j| \le 2\varepsilon_\kappa.$$

Then, it is analyzed that

$$\begin{aligned}\dot{\boldsymbol{\rho}}^{\mathrm{T}}\mathbf{M}\boldsymbol{\chi} =& \dot{\boldsymbol{\rho}}^{\mathrm{T}}\mathbf{M}^2\boldsymbol{\chi}\\ \le& ||\mathbf{M}\boldsymbol{\chi}||_1||\mathbf{M}\boldsymbol{\chi}||_1\\ \le& \max_{i,j}\{|\chi_i - \chi_j|\}\sum_{i=1}^{n}\sum_{j=1,j\neq i}^{n}\left|\dot{\tilde{\kappa}}_i - \dot{\tilde{\kappa}}_j\right|\\ \le& \max_{i,j}\{|\chi_i - \chi_j|\}\,n\max_i\left\{\sum_{j=1,j\neq i}^{n}\left|\dot{\tilde{\kappa}}_i - \dot{\tilde{\kappa}}_j\right|\right\}\\ \le& \frac{n\,(n-1)}{2}\max_{i,j}\{|\chi_i - \chi_j|\}\sum_{i=1}^{n}\sum_{j\in\boldsymbol{\mathcal{N}}_i}^{n}\left|\dot{\tilde{\kappa}}_i - \dot{\tilde{\kappa}}_j\right|\\ \le& n\,(n-1)\,\varepsilon_\kappa\sum_{i=1}^{n}\sum_{j\in\boldsymbol{\mathcal{N}}_i}^{n}\left|\dot{\tilde{\kappa}}_i - \dot{\tilde{\kappa}}_j\right|.\end{aligned}$$

Similarly, it has

$$\boldsymbol{\rho}^{\mathrm{T}}\mathbf{M}\boldsymbol{\chi} \le n\,(n-1)\,\varepsilon_\kappa\sum_{i=1}^{n}\sum_{j\in\boldsymbol{\mathcal{N}}_i}^{n}|\tilde{\kappa}_i - \tilde{\kappa}_j|.$$

We also know that

$$\varphi_\kappa\tilde{\boldsymbol{\kappa}}^{\mathrm{T}}\boldsymbol{\mathcal{H}}\mathrm{sgn}(\boldsymbol{\mathcal{H}}^{\mathrm{T}}\dot{\tilde{\boldsymbol{\kappa}}}) \le \varphi_\kappa\sum_{i=1}^{n}\sum_{j\in\boldsymbol{\mathcal{N}}_i}^{n}|\tilde{\kappa}_i - \tilde{\kappa}_j|.$$

Therefore, it follows that

$$\begin{aligned}\dot{V}_\kappa \le& -(a_\kappa - 1)\dot{\tilde{\boldsymbol{\kappa}}}^{\mathrm{T}}\dot{\tilde{\boldsymbol{\kappa}}} - b_\kappa\tilde{\boldsymbol{\kappa}}^{\mathrm{T}}\tilde{\boldsymbol{\kappa}}\\ &+ n\,(n-1)\,\varepsilon_\kappa\sum_{i=1}^{n}\sum_{j\in\boldsymbol{\mathcal{N}}_i}^{n}\left|\dot{\tilde{\kappa}}_i - \dot{\tilde{\kappa}}_j\right|\\ &+ n\,(n-1)\,\varepsilon_\kappa\sum_{i=1}^{n}\sum_{j\in\boldsymbol{\mathcal{N}}_i}^{n}|\tilde{\kappa}_i - \tilde{\kappa}_j| - \varphi_\kappa\sum_{i=1}^{n}\sum_{j\in\boldsymbol{\mathcal{N}}_i}\left|\dot{\tilde{\kappa}}_i - \dot{\tilde{\kappa}}_j\right|\\ &+ \varphi_\kappa\sum_{i=1}^{n}\sum_{j\in\boldsymbol{\mathcal{N}}_i}|\tilde{\kappa}_i - \tilde{\kappa}_j| - \pi_\kappa\sum_{i=1}^{n}\sum_{j\in\boldsymbol{\mathcal{N}}_i}|\tilde{\kappa}_i - \tilde{\kappa}_j|\\ \le& -(a_\kappa - 1)\dot{\tilde{\boldsymbol{\kappa}}}^{\mathrm{T}}\dot{\tilde{\boldsymbol{\kappa}}} - b_\kappa\tilde{\boldsymbol{\kappa}}^{\mathrm{T}}\tilde{\boldsymbol{\kappa}}\\ &- \left[\varphi_\kappa - n\,(n-1)\,\varepsilon_\kappa\right]\sum_{i=1}^{n}\sum_{j\in\boldsymbol{\mathcal{N}}_i}^{n}\left|\dot{\tilde{\kappa}}_i - \dot{\tilde{\kappa}}_j\right|\\ &- \left[\pi_\kappa - \varphi_\kappa - n\,(n-1)\,\varepsilon_\kappa\right]\sum_{i=1}^{n}\sum_{j\in\boldsymbol{\mathcal{N}}_i}^{n}|\tilde{\kappa}_i - \tilde{\kappa}_j|\\ \le& -\begin{bmatrix}\tilde{\boldsymbol{\kappa}}\\ \dot{\tilde{\boldsymbol{\kappa}}}\end{bmatrix}^{\mathrm{T}}\left(\begin{bmatrix}b_\kappa & 0\\ 0 & a_\kappa - 1\end{bmatrix}\right)\begin{bmatrix}\tilde{\boldsymbol{\kappa}}\\ \dot{\tilde{\boldsymbol{\kappa}}}\end{bmatrix}\\ &- \left[\pi_\kappa - \varphi_\kappa - n\,(n-1)\,\varepsilon_\kappa\right]\sum_{i=1}^{n}\sum_{j\in\boldsymbol{\mathcal{N}}_i}\int_0^{\tilde{\kappa}_i-\tilde{\kappa}_j}\mathrm{sgn}\,(s)ds\\ \le& -C_\kappa' V_\kappa,\end{aligned}$$

where

$$C_\kappa' = \min\left\{\frac{\pi_\kappa - \varphi_\kappa - n\,(n-1)\,\varepsilon_\kappa}{\pi_\kappa}, \frac{2\min\{a_\kappa - 1, b_\kappa\}}{\lambda_{\max}\left(\begin{bmatrix}a_\kappa + b_\kappa & 1\\ 1 & 1\end{bmatrix}\right)}\right\}.$$

This implies $\begin{bmatrix}\tilde{\boldsymbol{\kappa}} & \dot{\tilde{\boldsymbol{\kappa}}}\end{bmatrix} \to \boldsymbol{0}$. The formation scaling parameters reach an agreement. Then, we sum up the closed-loop dynamics of (15) and (16), yielding

$$\sum_{i=1}^{n} \ddot{\kappa}_i = \sum_{i=1}^{n} \ddot{\rho}_i - a_\kappa \sum_{i=1}^{n} (\dot{\kappa}_i - \dot{\rho}_i) - \beta_\kappa \sum_{i=1}^{n} (\kappa_i - \rho_i).$$

It apparently follows that $\sum_{i=1}^{n} \kappa_i \to \sum_{i=1}^{n} \rho_i$ and $\sum_{i=1}^{n} \dot{\kappa}_i \to \sum_{i=1}^{n} \dot{\rho}_i$, $t \to \infty$. In view of $\begin{bmatrix}\tilde{\boldsymbol{\kappa}} & \dot{\tilde{\boldsymbol{\kappa}}}\end{bmatrix} \to \boldsymbol{0}$, we know $\kappa_i \to \frac{1}{n}\sum_{j=1}^{n} \rho_j$ and $\dot{\kappa}_i \to \frac{1}{n}\sum_{j=1}^{n} \rho_j$, $t \to \infty$. Thus, the control objective is proved.

REFERENCES

[1] X. Zhang, F. Zhang, P. Huang et al., "Self-Triggered Based Coordinate Control with Low Communication for Tethered Multi-UAV Collaborative Transportation," *IEEE Robot. Autom. Lett.*, vol. 6, no. 2, pp. 1559-1566, 2021.

[2] K. Harikumar, J. Senthilnath and S. Sundaram, "Multi-UAV Oxyrrhis Marina-Inspired Search and Dynamic Formation Control for Forest Firefighting," *IEEE Trans. Autom. Sci. Eng.*, vol. 16, no. 2, pp. 863-873, 2019.

[3] A. Wallar, E. Plaku and D.A. Sofge, "Reactive Motion Planning for Unmanned Aerial Surveillance of Risk-Sensitive Areas," *IEEE Trans. Autom. Sci. Eng.*, vol. 12, no. 3, pp. 969-980, 2015.

[4] A. Guillet, R. Lenain, B. Thuilot, and V. Rousseau, "Formation Control of Agricultural Mobile Robots: A Bidirectional Weighted Constraints Approach," *J. F. Robot.*, vol. 34, no. 7, pp. 1260-1274, 2017.

[5] E. Gill, P. Sundaramoorthy, J. Bouwmeester, B. Zandbergen, and R. Reinhard, "Formation flying within a constellation of nano-satellites: The QB50 mission," *Acta Astronaut.*, vol. 82, no. 1, pp. 110-117, 2013.

[6] Y. Zhao, F. Zhang, P. Huang, and X. Liu, "Impulsive Super-Twisting Sliding Mode Control for Space Debris Capturing via Tethered Space Net Robot," *IEEE Trans. Ind. Electron.*, vol. 67, no. 8, pp. 6874-6882, 2020.

[7] Y. Wang, M. Shan, Y. Yue, and D. Wang, "Vision-based flexible leader-follower formation tracking of multiple nonholonomic mobile robots in unknown obstacle environments," *IEEE Trans. Control Syst. Technol.*, vol. 28, no. 3, pp. 1025-1033, 2020.

[8] X. Liu, S. S. Ge, and C. H. Goh, "Vision-Based Leader-Follower Formation Control of Multiagents with Visibility Constraints," *IEEE Trans. Control Syst. Technol.*, vol. 27, no. 3, pp. 1326-1333, 2019.

[9] F. Schiano and P. R. Giordano, "Bearing rigidity maintenance for formations of quadrotor UAVs," in *Proc. IEEE Int. Conf. Robot. Autom.*, pp. 1467-1474, 2017.

[10] R. Olfati-Saber, J. A. Fax, and R. M. Murray, "Consensus and cooperation in networked multi-agent systems," *Proc. IEEE*, vol. 95, no. 1, pp. 215-233, 2007.

[11] W. Ren, "Multi-vehicle consensus with a time-varying reference state," *Syst. Control Lett.*, vol. 56, no. 7-8, pp. 474-483, 2007.

[12] Z. Miao, Y. H. Liu, Y. Wang, G. Yi, and R. Fierro, "Distributed Estimation and Control for Leader-Following Formations of Nonholonomic Mobile Robots," *IEEE Trans. Autom. Sci. Eng.*, vol. 15, no. 4, pp. 1946-1954, 2018.

[13] S. P. Hou, C. C. Cheah, and J. J. E. Slotine, "Dynamic region following formation control for a swarm of robots," in *Proc. Int. Conf. Robot. Autom.*, 2009, pp. 1929-1934.

[14] J. Fu, Y. Lv, and W. Yu, "Robust adaptive time-varying region tracking control of multi-robot systems," *Sci. China Inf. Sci.*, vol. 66, no. 5, pp. 2022-2023, 2023.

[15] S. Coogan and M. Arcak, "Scaling the size of a formation using relative position feedback," *Automatica*, vol. 48, no. 10, pp. 2677-2685, 2012.

[16] Z. Han, G. Hu, L. Xie, and Z. Lin, "Estimation based formation control with size scaling for leader-follower networks," in *Proc. Int. Conf. Control. Autom. Robot. Vision*, 2018, pp. 1022-1027.

[17] Z. Han, L. Wang, Z. Lin, and R. Zheng, "Formation Control with Size Scaling Via a Complex Laplacian-Based Approach," *IEEE Trans. Cybern.*, vol. 46, no. 10, pp. 2348-2359, 2016.

[18] H. Garcia de Marina, "Distributed formation maneuver control by manipulating the complex Laplacian," *Automatica*, vol. 132, p. 109813, Oct. 2021.

[19] Q. Yang, Z. Sun, M. Cao, H. Fang, and J. Chen, "Construction of universally rigid tensegrity frameworks and their applications in formation scaling control," in *Proc. Chin. Control Conf.*, 2017, pp. 8177-8182.

[20] Q. Yang, M. Cao, Z. Sun, H. Fang, and J. Chen, "Formation scaling control using the stress matrix," in *Proc. Annu. Conf. Decis. Control*, 2018, pp. 3449-3454.

[21] Q. Yang, H. Fang, M. Cao, and J. Chen, "Planar Affine Formation Stabilization via Parameter Estimations," *IEEE Trans. Cybern.*, vol. 52, no. 6, pp. 5322-5332, Jun. 2022.

[22] Q. Yang, Z. Sun, M. Cao, H. Fang, and J. Chen, "Stress-matrix-based formation scaling control," *Automatica*, vol. 101, pp. 120-127, 2019.

[23] J. Wang, X. Ding, C. Wang, Z. Zuo, and Z. Ding, "Affine Formation Control of General Linear Multi-Agent Systems with Delays," *Unmanned Syst.*, vol. 11, no. 02, pp. 123-132, Apr. 2023.

[24] O. Onuoha, H. Tnunay, Z. Li, and Z. Ding, "Affine Formation Algorithms and Implementation Based on Triple-Integrator Dynamics," *Unmanned Syst.*, vol. 7, no. 1, pp. 33-45, Jan. 2019.

[25] S. Zhao and D. Zelazo, "Translational and scaling formation maneuver control via a bearing-based approach," *IEEE Trans. Control Netw. Syst.*, vol. 4, no. 3, pp. 429-438, 2017.

[26] Y. Lu, C. Wen, T. Shen, and W. Zhang, "Bearing-Based Adaptive Neural Formation Scaling Control for Autonomous Surface Vehicles with Uncertainties and Input Saturation," *IEEE Trans. Neural Networks Learn. Syst.*, vol. 32, no. 10, pp. 4653-4664, 2021.

[27] I. Buckley and M. Egerstedt, "Infinitesimal Shape-Similarity for Characterization and Control of Bearing-Only Multirobot Formations," *IEEE Trans. Robot.*, vol. 37, no. 6, pp. 1921-1935, 2021.

[28] R. A. Freeman, P. Yang, and K. M. Lynch, "Stability and convergence properties of dynamic average consensus estimators," in *Proc. IEEE Conf. Decis. Control*, Dec. 2006, pp. 398-403.

[29] F. Chen, W. Ren, W. Lan, and G. Chen, "Distributed average tracking for reference signals with bounded accelerations," *IEEE Trans. Automat. Contr.*, vol. 60, no. 3, pp. 863-869, 2015.

[30] S. Ghapani, S. Rahili, and W. Ren, "Distributed Average Tracking of Physical Second-Order Agents with Heterogeneous Unknown Nonlinear Dynamics Without Constraint on Input Signals," *IEEE Trans. Automat. Contr.*, vol. 64, no. 3, pp. 1178-1184, 2019.

[31] M. Saim, S. Ghapani, W. Ren, K. Munawar, and U. M. Al-Saggaf, "Distributed average tracking in multi-agent coordination: Extensions and experiments," *IEEE Syst. J.*, vol. 12, no. 3, pp. 2428-2436, 2018.

[32] F. Chen and W. Ren, "A Connection between Dynamic Region-Following Formation Control and Distributed Average Tracking," *IEEE Trans. Cybern.*, vol. 48, no. 6, pp. 1760-1772, 2018.

[33] F. Chen, Y. Cao, and W. Ren, "Distributed average tracking of multiple time-varying reference signals with bounded derivatives," *IEEE Trans. Automat. Contr.*, vol. 57, no. 12, pp. 3169-3174, 2012.

[34] C. Yu, H. Wang, and W. Yu, "Distributed Average Tracking Problem Under Directed Networks: A Distributed Estimator-Based Design," *IEEE Trans. Control Netw. Syst.*, vol. 9, no. 2, pp. 930-942, Jun. 2022.

[35] H. Hong, G. Wen, X. Yu, and W. Yu, "Robust Distributed Average Tracking for Disturbed Second-Order Multiagent Systems," *IEEE Trans. Syst. Man, Cybern. Syst.*, vol. 52, no. 5, pp. 3187-3199, May 2022.

[36] A. D. Ames, X. Xu, J. W. Grizzle, and P. Tabuada, "Control Barrier Function Based Quadratic Programs for Safety Critical Systems," *IEEE Trans. Automat. Contr.*, vol. 62, no. 8, pp. 3861-3876, 2017.

[37] W. Xiao and C. Belta, "High-Order Control Barrier Functions," *IEEE Trans. Automat. Contr.*, vol. 67, no. 7, pp. 3655-3662, Jul. 2022.

[38] W. Xiao and C. Belta, "Control Barrier Functions for Systems with High Relative Degree,in *Proc. IEEE Conf. Decis. Control*, Dec. 2019, pp. 474-479.

[39] J. Breeden and D. Panagou, "High Relative Degree Control Barrier Functions Under Input Constraints," in *Proc. IEEE Conf. Decis. Control*, Dec. 2021, pp. 6119-6124.

[40] X. Xu, "Control sharing barrier functions with application to constrained control," in *Proc. IEEE Conf. Decis. Control*, Dec. 2016, pp. 4880-4885.

[41] X. Xu, "Constrained control of inputoutput linearizable systems using control sharing barrier functions," *Automatica*, vol. 87, pp. 195-201, 2018.

[42] N. Biggs, *Algebraic Graph Theory, Cambridge Tracks in Mathematics.* Cambridge, U.K.: Cambridge Univ. Press, 1974.

[43] H. N. Nguyen, S. Park, J. Park, and D. Lee, "A Novel Robotic Platform for Aerial Manipulation Using Quadrotors as Rotating Thrust Generators," *IEEE Trans. Robot.*, vol. 34, no. 2, pp. 353-369, 2018.

[44] Y. Tian et al., "Search and rescue under the forest canopy using multiple UAVs," *Int. J. Rob. Res.*, vol. 39, no. 1011, pp. 1201-1221, 2020.

Xiaozhen Zhang received M.S. degree in navigation, guidance and control, from Northwestern Polytechnical University, Xian, China, in 2021. He is currently working toward the Ph.D. degree in control engineering at Beijing Institute of Technology, Beijing, China.

His research interests include robotics, formation planning, formation control and multi-agent systems.

Qingkai Yang (Member, IEEE) received the first Ph.D. degree in control science and engineering from the Beijing Institute of Technology, Beijing, China, in 2018, and the second Ph.D. degree in system control from the University of Groningen, Groningen, The Netherlands, in 2018.

He is currently an Associate Professor with the School of Automation, Beijing Institute of Technology. His research interest is in formation control of multi-agent systems and autonomous agents.

Jingshuo Lyu received the B.S. degree in automation from the Beijing Institute of Technology, Beijing, China, in 2021, and is currently pursuing the M.S. degree in control science and engineering from the Beijing Institute of Technology, Beijing, China.

His research interests include tensegrity robotics, motion planning and air-ground amphibious robot.

Xinyue Zhao received the B.S. degree in automation from the Shenyang Ligong University, Shenyang, China, in 2019, and is currently pursuing the Ph.D. degree in control science and engineering from the Beijing Institute of Technology, Beijing, China.

His research interests include safe control of multi-agent systems, distributed optimization, formation control, and control applications.

Hao Fang (Member, IEEE) received the B.S. degree from the Xian University of Technology, Shaanxi, China, in 1995, and the M.S. and Ph.D. degrees from the Xian Jiaotong University, Shaanxi, in 1998 and 2002, respectively.

Since 2011, he has been a Professor with the Beijing Institute of Technology, Beijing, China. He held two postdoctoral appointments with the INRIA/France Research Group of COPRIN and the LASMEA (UNR6602 CNRS/Blaise Pascal University, Clermont-Ferrand, France).

His research interests include all-terrain mobile robots, robotic control, and multiagent systems.